AD_____

Award Number: W81XWH-12-1-0153

TITLE: Probing Androgen Receptor Signaling in Circulating Tumor Cells in Prostate Cancer

PRINCIPAL INVESTIGATOR: David T. Miyamoto, M.D., Ph.D.

CONTRACTING ORGANIZATION: Massachusetts General Hospital
Boston, MA 02114-2621

REPORT DATE: July 2013

TYPE OF REPORT: Annual Summary

PREPARED FOR: U.S. Army Medical Research and Materiel Command
Fort Detrick, Maryland 21702-5012

REPORT DOCUMENTATION PAGE

Form Approved
OMB No. 0704-0188

1. REPORT DATE	2. REPORT TYPE	3. DATES COVERED
July 2013	Annual Summary	1 July 2012 – 30 June 2013

4. TITLE AND SUBTITLE

Probing Androgen Receptor Signaling in Circulating Tumor Cells in Prostate Cancer

5a. CONTRACT NUMBER

5b. GRANT NUMBER
W81XWH-12-1-0153

5c. PROGRAM ELEMENT NUMBER

6. AUTHOR(S)

David T. Miyamoto, M.D., Ph.D.

E-Mail: dmiyamoto@partners.org

5d. PROJECT NUMBER

5e. TASK NUMBER

5f. WORK UNIT NUMBER

7. PERFORMING ORGANIZATION NAME(S) AND ADDRESS(ES)

Massachusetts General Hospital
Boston, MA 02114-2621

8. PERFORMING ORGANIZATION REPORT NUMBER

9. SPONSORING / MONITORING AGENCY NAME(S) AND ADDRESS(ES)
U.S. Army Medical Research and Materiel Command
Fort Detrick, Maryland 21702-5012

10. SPONSOR/MONITOR'S ACRONYM(S)

11. SPONSOR/MONITOR'S REPORT NUMBER(S)

12. DISTRIBUTION / AVAILABILITY STATEMENT
Approved for Public Release; Distribution Unlimited

13. SUPPLEMENTARY NOTES

14. ABSTRACT

This Award focuses on using a novel microfluidic "CTC-chip" to capture and measure androgen receptor (AR) activity in circulating tumor cells (CTCs) in prostate cancer patients before and after hormonal therapy. During the first year of this award, we have successfully developed a quantitative immunofluorescence assay to measure AR activity in single CTCs, and have piloted this assay in men with metastatic prostate cancer receiving treatment with hormonal therapy. Preliminary results suggest that this novel assay can effectively measure AR activity levels in CTCs, and that CTC AR activity at baseline and after therapy may be correlated with treatment outcomes. Thus, this CTC-based assay may serve as a non-invasive biomarker that can potentially help guide therapy in prostate cancer. These initial results were published during this term in Cancer Discovery. Ongoing efforts include single CTC transcriptional profiling to better understand heterogeneity of metastatic precursor cells and uncover alternative signaling pathways that may be activated in castration-resistant prostate cancer.

15. SUBJECT TERMS
prostate cancer, circulating tumor cells, androgen receptor, castration-resistant prostate cancer, RNA sequencing, single cell

16. SECURITY CLASSIFICATION OF:			17. LIMITATION OF ABSTRACT	18. NUMBER OF PAGES	19a. NAME OF RESPONSIBLE PERSON
a. REPORT	b. ABSTRACT	c. THIS PAGE			USAMRMC
U	U	U	UU	38	19b. TELEPHONE NUMBER *(include area code)*

Table of Contents

Page

INTRODUCTION

Castration-resistant prostate cancer (CRPC) is thought to arise from the persistence of androgen receptor (AR) signaling in cancer cells despite castrate levels of testosterone (1). In this Research Project, we use a novel microfluidic technology (the "CTC-chip") to interrogate the status of AR signaling activity in circulating tumor cells (CTCs) isolated from metastatic prostate cancer patients. An AR activity signature developed in prostate cancer cell lines is being applied to CTCs in patients with castration-resistant prostate cancer (CRPC) before and after secondary hormonal therapies to test the hypothesis that effective suppression of AR signaling in CTCs correlates with clinical response to hormonal therapy. To identify novel genes and pathways involved in the evolution of castration-resistant disease, digital gene expression profiling of CTCs is being performed. These studies are aimed at providing initial validation of a novel molecular biomarker that can monitor and predict responses to second-line hormonal therapy in patients with CRPC, as well as revealing fundamental insights into the mechanisms underlying castration-resistance in prostate cancer. Progress during Year 1 of this Research Project includes development of a single cell immunofluorescence-based assay for measurement of AR activity; demonstration of the feasibility of using AR activity in CTCs as a biomarker to monitor and potentially predict response to second line hormonal therapy in a small cohort of patients with CRPC; and the demonstration of feasibility of performing high throughput qRT-PCR and whole transcriptome RNA-sequencing of single prostate CTCs. These pilot studies have resulted in two published manuscripts so far, attached in the Appendix to this report. Ongoing studies are aimed at further validation of the CTC AR activity assay in additional patients, and on transcriptional profiling analysis of single CTCs to provide insights into the molecular mechanisms of the development of CRPC.

SPECIFIC AIMS

1. Define an AR activity score in CTCs and test the hypothesis that AR signaling activity in prostate CTCs correlates with response to second-line hormonal therapy in metastatic prostate cancer patients.

2. Perform digital gene expression (DGE) profiling of prostate CTCs to identify novel pathways that promote castration resistance.

BODY

Progress on Statement of Work (SOW) During this Reporting Period.

This Research Project uses a novel microfluidic technology called the "CTC-chip" to interrogate the status of androgen receptor (AR) signaling activity in circulating tumor cells (CTCs) isolated from metastatic prostate cancer patients (2). An AR activity signature developed in prostate cancer cell lines is being applied to CTCs in patients with castration-resistant prostate cancer (CRPC) before and after secondary hormonal therapy to test the hypothesis that effective suppression of AR signaling in CTCs correlates with clinical response to hormonal therapy. To identify novel genes and pathways involved in the evolution of castration-resistant disease, digital gene expression profiling of CTCs is being performed. Progress on Tasks related to the Research Project are outlined below.

Task 1. Regulatory review and approval of clinical protocol.

A clinical research protocol for the collection of blood from patients with solid tumors for CTC analysis (DF/HCC 05-300) was initially received by the US Army Medical Research and Materiel Command (USAMRMC), Office of Research Protections (ORP), Human Research Protection Office (HRPO) on 9 May 2012, and reviewed for compliance with human subject protection requirements. A revised research consent form and clinical research protocol was approved by the HRPO on 7 June 2012, and this revised protocol was approved by the Dana-Farber Cancer Institute Institutional Review Board (DFCI IRB) on 12 July 2012. This final protocol then received approval by the HRPO on 30 July 2012. Continuation of the subject protocol was approved by the DFCI IRB on 30 May 2013, and was in turn approved by the HRPO on 19 July 2013. This approval is due for continuing review by the DFCI IRB on 30 May 2014.

Task 2. (Aim 1) Recruitment of patients with castration-resistant prostate cancer for CTC AR activity analysis.

Thus far, 17 patients with CRPC have been recruited for the purposes of AR activity analysis in CTCs through the DF/HCC 05-300 clinical protocol described above. Interim results from CTC AR activity analysis from these patients are described below.

Task 3. (Aim 1) CTC AR signature activity analysis in patients.

As second line AR targeting therapies enter clinical care for CRPC (e.g. abiraterone acetate and enzalutamide) in addition to cytotoxic therapeutics (e.g. docetaxel, cabazitaxel, Ra-223), no reliable biomarkers exist to target appropriate therapies to individual patients (3, 4). To address this challenge, we developed a single cell immunophenotyping approach to measure AR activity in CTCs using two genes that we identified as most consistently upregulated and downregulated following AR modulation in prostate cancer cells: PSA (androgen driven) and PSMA (androgen suppressed). While developing and testing our two color assay using androgen responsive prostate cancer cell lines, we effectively identified PSA+/PSMA- cells as androgen activated (AR-on) and PSA-/PSMA+ cells as androgen suppressed (AR-off). In transition between AR-on and AR-off states, we identified PSA+/PSMA+ (AR-mixed) cells.

Application of this CTC-based assay in a small cohort of men with prostate cancer revealed several interesting findings. In treatment-naïve men with metastatic prostate cancer, the majority of CTCs were AR-on. Within 4 weeks of initiation of androgen deprivation therapy, these CTCs turned predominantly to AR-off, and CTC counts thereafter dropped below

detection. In contrast, striking heterogeneity was evident in CRPC where some patients had only AR-on cells, some had only AR-off cells, and others had large numbers of dual positive AR-mixed cells. In a cohort of 17 patients with CRPC treated with abiraterone acetate, the presence of AR-mixed cells prior to treatment or an increase in AR-on cells despite therapy were associated with decreased overall survival. Together, these studies point to a novel approach to measure the fraction of CTCs that are AR-driven and likely to be sensitive to hormonal therapy. These preliminary results are described in detail in the manuscript attached in the appendix (Miyamoto et al., Cancer Discovery 2012), which was published during this reporting period (5).

In our future plans, we plan to initiate a larger-scale clinical trial to validate this assay in additional castration-resistant prostate cancer patients receiving second-line hormonal therapy, with the hope that it will prove useful in directing individualized therapies for castration-resistant disease.

Task 4. (Aim 2) Recruitment of patients with metastatic castration-resistant prostate cancer and metastatic castration-sensitive prostate cancer for digital gene expression profiling.

Thus far, 17 patients with CRPC and 3 patients with CSPC have been recruited for the purposes of digital gene expression profiling of CTCs through the DF/HCC 05-300 clinical protocol described above. Interim results from digital gene expression profiling of these patients is described below.

Task 5. (Aim 2) Digital gene expression profiling of CTCs including sample preparation and RNA sequencing.

One of our primary goals is to identify cellular pathways that underlie the acquisition of castration-resistance by dissecting the transcriptome of CTCs. Reactivation of AR signaling by itself cannot fully explain castration resistant disease, given the relatively modest clinical benefit of second line hormonal therapies, as well as the evident heterogeneity of androgen signaling readouts that we have uncovered through quantitative immunofluorescence PSA/PSMA single cell immunophenotyping described above (5). However, given this intercellular heterogeneity, defining the relevant signaling pathways will require RNA sequencing and digital gene expression profiling at the level of individual single CTCs. The use of single CTC analysis also obviates the need for digital subtraction of contaminating leukocyte signal that has been necessary with RNA sequencing of preparations of whole CTC/leukocyte mixtures (6).

During this reporting period, we have piloted the use of a third generation CTC-chip (CTC-iChip) recently designed at the MGH, which is capable of generating high purity CTC preparations in solution that can be micromanipulated for single cell analysis (7). As proof of principle to demonstrate our ability to micromanipulate single CTCs and extract high quality RNA for molecular analyses, we used the CTC-iChip to isolate 15 CTCs from a patient with metastatic CRPC and performed microfluidic qRT-PCR for a panel of 43 genes. These results are described in detail in the manuscript attached in the appendix (Ozkumur et al., Science Translational Medicine 2013), specifically in Figure 7 of the manuscript, which was published during this reporting period (7). This initial analysis has set the stage for our subsequent analyses using RNA sequencing of individual prostate CTCs.

We have subsequently established protocols in our lab for single CTC RNA-sequencing by adapting methods published previously for single cell RNA-sequencing of single mouse blastomeres (8). In the single cell context (as opposed to CTC/leukocyte mixtures), PCR

amplification of signal is essential and does not carry the risk of loss of CTC signal, hence the single molecule Helicos sequencing platform is not required. We are using the ABI SOLiD 5500 library preparation procedures, including reverse transcription, sonication to fragments of 80-130bp, end repair, blunt-end ligation and emulsion PCR, followed by Next Generation Sequencing using the ABI SOLiD 5500 machines provided by the MGH Center for Cancer Research Core facility (8). To date, we have piloted this approach with 30 single CTCs from 6 CRPC patients and have derived RNA sequencing reads that are comparable to those with control cancer cell lines, with an average of 9,508,135 reads per cell and 5,005,694 reads aligned to the known transcriptome per cell, providing approximately 10-20x coverage (Fig. 1). We plan to continue applying this single cell RNA sequencing protocol to 100 individual CTCs from patients with castration resistant compared to castration sensitive prostate cancer.

***Figure 1**: (A) Heat map of whole transcriptome RNA-seq digital gene expression profiles for 30 single prostate CTCs isolated from 6 different CRPC patients. (B) Close up of selected key gene groupings, demonstrating high expression of prostate-specific and epithelial genes, and minimal expression of hematopoietic genes. (Miyamoto et al., unpublished)*

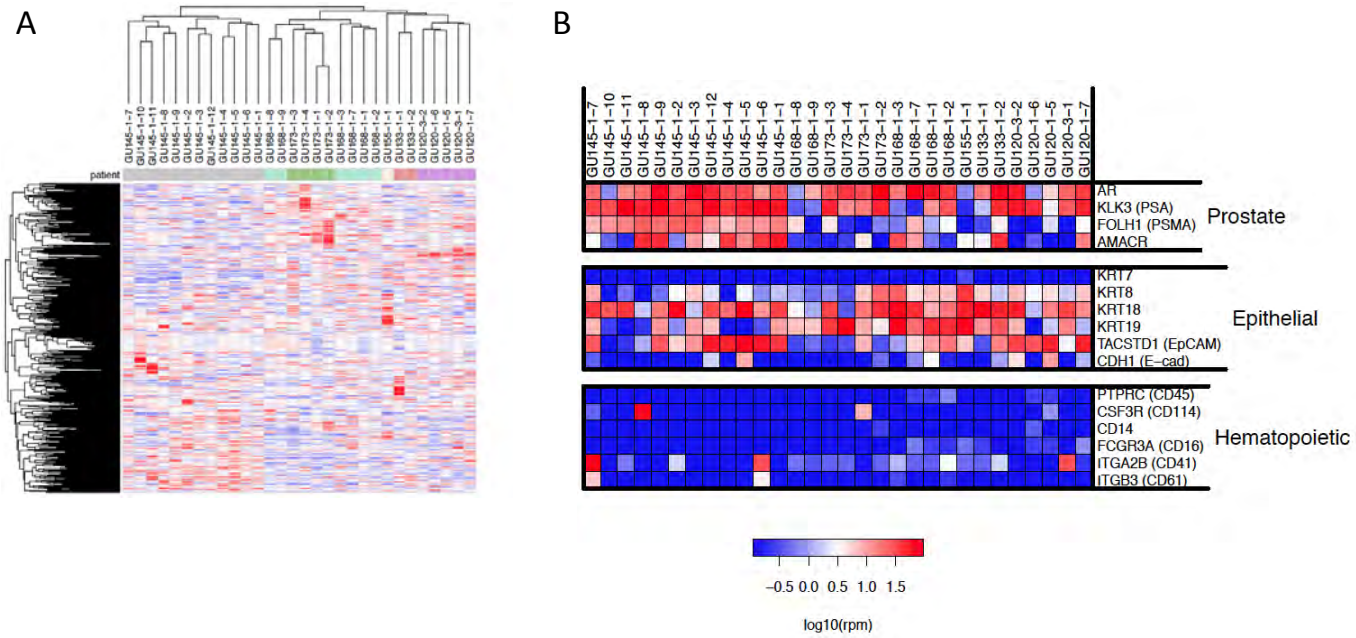

Task 6. (Aim 2) Data analysis of CTC digital gene expression profiles.

Using the above strategy for single cell RNA-sequencing, we will analyze the digital gene expression profiles of single CTCs isolated from patients with castration resistant compared to castration sensitive prostate cancer. We will attempt to address two primary questions: 1. What is the heterogeneity of CTCs, and is there a subset with expression profiles that may be consistent with distinct metastatic precursors/cancer stem cell phenotypes? 2. What are the signaling pathways activated in individual cells from patients with castration resistant prostate cancer, and do they identify potential drug targets that could be combined with hormonal therapies to suppress metastasis in advanced prostate cancer? These analyses are currently in the preliminary stages, and progress will be described in the next reporting period.

Task 7. (Aim 2) Validation and follow-up studies of promising genes and pathways identified through CTC digital gene expression profiles.

Progress on this Task will be reported after we have identified candidate genes and pathways involved in castration-resistant prostate cancer through analysis of CTC digital gene expression profiles, obtained through the methods described above.

Task 8. Preparation of results, presentations, and manuscripts.

We have published a manuscript in *Cancer Discovery* during this reporting period describing our preliminary results analyzing AR signaling activity in CTCs using the PSA/PSMA immunfluorescence-based assay (attached in the Appendix) (5). In addition, pilot data demonstrating the isolation of single CTCs using the CTC-iChip followed by microfluidic multigene qRT-PCR was published as part of a manuscript in *Science Translational Medicine* during this reporting period (attached in the Appendix) (7). Finally, several presentations were delivered during this reporting period, including a departmental seminar at the MGH Cancer Center in December 2012 and an oral presentation at the BIO International Convention in Chicago, IL in April 2013. It is anticipated that several additional manuscripts will be published during the term of this Research Project.

KEY RESEARCH ACCOMPLISHMENTS

- Development of an androgen receptor (AR) signaling assay in CTCs based on a two-color PSA/PSMA immunofluorescence assay.
- Preliminary demonstration of the ability of the immunofluorescence-based AR signaling assay to measure AR activity in CTCs in patients with prostate cancer, and potentially predict patient outcomes after abiraterone acetate treatment.
- Development of a methodology to isolate single CTCs for RNA analysis using the microfluidic CTC-iChip.
- Demonstration of the feasibility of microfluidic qRT-PCR to measure mRNA transcript levels in single prostate CTCs.
- Demonstration of feasibility of RNA-sequencing and digital gene expression profiling of whole transcriptomes in single prostate CTCs.

REPORTABLE OUTCOMES

- Manuscripts:
    - **Miyamoto, D.T.,** Lee, R.J., Stott, S.L., Ting, D.T., Wittner, B.S., Ulman, M., Smas, M.E., Lord, J.B., Brannigan, B.W., Trautwein, J., Bander, N.H., Wu, C.L., Sequist, L.V., Smith, M.R., Ramaswamy, S., Toner, M., Maheswaran, S., Haber, D.A. (2012). Androgen receptor signaling in circulating tumor cells as a marker of hormonally responsive prostate cancer. *Cancer Discovery*, 2:995-1003*.*

    - Ozkumur, E., Shah, A.M., Ciciliano, J.C., Emmink, B.L., **Miyamoto, D.T.**, Brachtel, E., Yu, M., Chen, P., Morgan, B., Trautwein, J., Kimura, A., Sengupta, S., Stott, S.L., Karabacak, N.M., Barber, T.A., Walsh, J.R., Smith, K., Spuhler, P., Sullivan, J., Lee, R., Ting, D.T., Luo, X., Shaw, A.T., Bardia, A., Sequist, L.V., Louis, D.N., Maheswaran, S., Kapur, R., Haber, D.A., Toner, M. (2013). Inertial Focusing for Positive and Negative Sorting of Rare Circulating Tumor Cells. *Science Translational Medicine,* 5:179ra47*.*

- Presentations:
    - **Miyamoto, D.T.** "Monitoring Androgen Receptor Signaling in Circulating Tumor Cells in Prostate Cancer." Departmental Seminar, MGH Cancer Center, Massachusetts General Hospital, Boston, MA 12 December 2012.

    - **Miyamoto, D.T.** "Microfluidic Isolation and Molecular Analysis of Circulating Tumor Cells." BIO International Convention, Chicago, IL, 22 April 2013.

CONCLUSION

During this reporting period, we have made considerable progress in demonstrating the use a novel microfluidic technology (the "CTC-chip") to isolate circulating tumor cells (CTCs) from metastatic prostate cancer patients, interrogate their AR signaling activity, and perform RNA-sequencing to identify genes and pathways involved in the evolution of castration-resistant prostate cancer (CRPC). Progress during Year 1 of this Research Project includes development of a single cell immunofluorescence-based assay to measure AR activity;

demonstration of feasibility of using AR activity in CTCs as a biomarker to monitor and potentially predict response to second line hormonal therapy in patients with CRPC; and demonstration of feasibility of performing high throughput qRT-PCR and whole transcriptome RNA-sequencing of single prostate CTCs. Ongoing efforts are aimed at further validation of the CTC AR activity assay in additional patients, and transcriptional profiling analysis of single CTCs from patients with castration-resistant and castration-sensitive prostate cancer. If successful, this Research Project will provide initial validation of a novel molecular biomarker that can monitor and predict responses to second-line hormonal therapy in patients with CRPC, as well as reveal fundamental insights into the mechanisms underlying castration-resistance in prostate cancer.

REFERENCES

1. Chen Y, Clegg NJ, Scher HI. Anti-androgens and androgen-depleting therapies in prostate cancer: new agents for an established target. Lancet Oncol 2009; 10: 981-91.
2. Stott SL, Hsu CH, Tsukrov DI, Yu M, Miyamoto DT, Waltman BA, et al. Isolation of circulating tumor cells using a microvortex-generating herringbone-chip. Proc Natl Acad Sci U S A 2010; 107: 18392-7.
3. de Bono JS, Logothetis CJ, Molina A, Fizazi K, North S, Chu L, et al. Abiraterone and increased survival in metastatic prostate cancer. N Engl J Med 2011; 364: 1995-2005.
4. Scher HI, Fizazi K, Saad F, Taplin ME, Sternberg CN, Miller K, et al. Increased survival with enzalutamide in prostate cancer after chemotherapy. N Engl J Med 2012; 367: 1187-97.
5. Miyamoto DT, Lee RJ, Stott SL, Ting DT, Wittner BS, Ulman M, et al. Androgen receptor signaling in circulating tumor cells as a marker of hormonally responsive prostate cancer. Cancer Discov 2012; 2: 995-1003.
6. Yu M, Ting DT, Stott SL, Wittner BS, Ozsolak F, Paul S, et al. RNA sequencing of pancreatic circulating tumour cells implicates WNT signalling in metastasis. Nature 2012; 487: 510-3.
7. Ozkumur E, Shah AM, Ciciliano JC, Emmink BL, Miyamoto DT, Brachtel E, et al. Inertial focusing for tumor antigen-dependent and -independent sorting of rare circulating tumor cells. Sci Transl Med 2013; 5: 179ra47.
8. Tang F, Barbacioru C, Wang Y, Nordman E, Lee C, Xu N, et al. mRNA-Seq whole-transcriptome analysis of a single cell. Nat Methods 2009; 6: 377-82.

APPENDICES

Includes the following: **Page**

BIOGRAPHICAL SKETCH

Provide the following information for the Senior/key personnel and other significant contributors in the order listed on Form Page 2.
Follow this format for each person. **DO NOT EXCEED FOUR PAGES.**

NAME	POSITION TITLE
Miyamoto, David T.	Instructor in Radiation Oncology, Harvard Medical School Assistant Physician, Massachusetts General Hospital
eRA COMMONS USER NAME (credential, e.g., agency login)	

EDUCATION/TRAINING *(Begin with baccalaureate or other initial professional education, such as nursing, include postdoctoral training and residency training if applicable.)*

INSTITUTION AND LOCATION	DEGREE *(if applicable)*	MM/YY	FIELD OF STUDY
Harvard College, Cambridge, MA	A.B.	06/1997	Chemistry
Harvard University, Cambridge, MA	Ph.D.	11/2004	Cell & Developmental Biology
Harvard Medical School, Boston, MA	M.D.	06/2006	Medicine
Brigham & Women's Hospital, Boston, MA		06/2007	Intern, Internal Medicine
Harvard Radiation Oncology Program, Boston, MA		06/2011	Resident, Radiation Oncology

A. Personal Statement

My multidisciplinary training in molecular cell biology, clinical radiation oncology, and prostate cancer biology has enabled me to become a translational physician scientist with a strong clinical and research interest in prostate cancer. I received my MD-PhD working in the laboratory of Dr. Timothy Mitchison studying the mechanisms of mitosis. I began postdoctoral research in circulating tumor cells in prostate cancer with Dr. Daniel Haber while completing my radiation oncology clinical training. I am currently an Instructor in Radiation Oncology at Harvard Medical School, devoting 80% of my effort to translational research in prostate cancer and 20% to clinical activities treating patients with genitourinary malignancies.

B. Positions and Honors

Positions and Employment

2009 -	Postdoctoral Research Fellow, Massachusetts General Hospital Cancer Center / Howard Hughes Medical Institute, Boston, MA (Professor Daniel A. Haber)
2011 -	Instructor in Radiation Oncology, Harvard Medical School
2011 -	Assistant Physician in Radiation Oncology, Massachusetts General Hospital

Other Professional Positions

1999 - 2006	Resident Tutor in Medicine, Leverett House, Harvard College, Cambridge, MA
2007	Visiting Physician, National Cancer Center Hospital, Tokyo, Japan
2011 -	Harvard-MIT Health Sciences and Technology MD Board of Advisors, Harvard Medical School

Academic and Professional Honors

1993	National Merit Scholarship
1993 – 1997	John Harvard Scholarship
1996	Merck Undergraduate Research Fellow
1997	*Magna cum laude*, Harvard College
1997	High Honors in Chemistry, Harvard College
2001 – 2004	Howard Hughes Medical Institute Predoctoral Fellow
2009 – 2011	B. Leonard Holman Research Pathway, American Board of Radiology
2010	ASTRO Annual Meeting Scientific Abstract Award
2011 – 2013	A. David Mazzone Career Development Award, Dana-Farber/Harvard Cancer Center
2011 – 2012	Research Career Development Award, Federal Share of the Proton Beam, NCI/MGH
2012 – 2017	Physician Research Training Award, Department of Defense

Licensure and Certification

2008 – present Massachusetts Full License, Board of Registration in Medicine
2012 – present Board Certification, Radiation Oncology, American Board of Radiology

Membership in Professional Societies

2003 – present Member, American Society for Cell Biology
2013 – present Member, American Association for Cancer Research
2008 – present Member, American Society for Radiation Oncology
2008 – present Member, Radiological Society of North America
2009 – present Member, American Society of Clinical Oncology

C. Selected Peer-reviewed Publications

Peer-reviewed articles

1. Haggarty, S.J., Mayer, T.U., **Miyamoto, D.T.**, Fathi, R., King, R.W., Mitchison, T.J., and Schreiber, S.L. (2000). Dissecting cellular processes using small molecules: identification of colchicine-, taxol-like, and other small molecules that perturb mitosis. *Chemistry & Biology*, 7:275-86.
2. McDonald, W.H., Ohi, R., **Miyamoto, D.T.**, Mitchison, T.J., and Yates, J.R. 3rd. (2002). Comparison of three directly coupled HPLC MS/MS strategies for identification of proteins from complex mixtures: single-dimensional LC-MS/MS, 2-phase MudPIT, and 3-phase MudPIT. *International Journal of Mass Spectrometry*, 219:245-51.
3. Gupta, A., Sanada, K., **Miyamoto, D.T.**, Rovelstad, S., Nadarajah, B., Pearlman, A.L., Brunstrom, J., and Tsai, L.-H. (2003). Layering defect in p35 deficiency is linked to improper neuronal-glial interaction in radial migration. *Nature Neuroscience*, 6:1284-91.
4. Groen, A.C., Cameron, L.A., Coughlin, M., **Miyamoto, D.T.**, Mitchison, T.J., and Ohi, R. (2004). XRHAMM functions in Ran-dependent microtubule nucleation and pole formation during anastral spindle assembly. *Current Biology*, 14:1801-11.
5. **Miyamoto, D.T.**, Perlman, Z.E., Burbank, K.S., Groen, A.C., and Mitchison, T.J. (2004). The kinesin Eg5 drives poleward microtubule flux in *Xenopus* egg extract spindles. *The Journal of Cell Biology*, 167:813-8.
6. Mak, R.H., Mamon, H.J., Ryan, D.P., **Miyamoto, D.T.**, Ancukiewicz, M.**,** Kobayashi, W.K., Willett, C.G., Choi, N.C., Blaszkowsky, L.S., Hong, T.S. (2010). Toxicity and outcomes after chemoradiation for esophageal cancer in patients age 75 or older. *Diseases of the Esophagus*, 23:316-23. Epub 2009 Sep 24.
7. **Miyamoto, D.T.**, Mamon, H.J., Ryan, D.P., Willett, C.G., Ancukiewicz, M., Kobayashi, W., Fernandez del Castillo, C., Blaszkowsky, L., Hong, T.S. (2010). Outcomes and tolerability of chemoradiation therapy for pancreatic cancer patients aged 75 years or older. *International Journal of Radiation Oncology, Biology, Physics*, 77:1171-7. Epub 2009 Sep 30.
8. Stott, S.L., Lee, R.J., Nagrath, S., Yu, M., **Miyamoto, D.T.**, Ulkus, L., Inserra, E.J., Ulman, M., Springer, S., Nakamura, Z., Moore, A.L., Tsukrov, D.I., Kempner, M.E., Dahl, D.M., Wu, C., Iafrate, A.J., Smith, M.R., Tompkins, R.G., Sequist, L.V., Toner, M., Haber, D.A., Maheswaran, S. (2010). Microfluidic isolation and molecular characterization of circulating tumor cells from patients with localized and metastatic prostate cancer. *Science Translational Medicine*, 2:25ra23:1-10.
9. Stott, S.L., Hsu, C.H., Tsukrov, D., Yu, M., **Miyamoto, D.T.**, Waltman, B.A., Rothenberg, S.M., Shah, A.M., Smas, M.E., Korir, G., Floyd, F.P., Gilman, A., Lord, J.B., Winokur, D., Nagrath, S., Sequist, L.V., Lee, R.J., Isselbacher, K.J., Maheswaran, S., Haber, D.A., Toner, M. (2010). Isolation of circulating tumor cells using a microvortex-generating herringbone-chip. *Proceedings of the National Academy of Sciences U.S.A.*, 107:18392-7.
10. **Miyamoto, D.T.,** Lee, R.J., Stott, S.L., Ting, D.T., Wittner, B.S., Ulman, M., Smas, M.E., Lord, J.B., Brannigan, B.W., Trautwein, J., Bander, N.H., Wu, C.L., Sequist, L.V., Smith, M.R., Ramaswamy,

S., Toner, M., Maheswaran, S., Haber, D.A. (2012). Androgen receptor signaling in circulating tumor cells as a marker of hormonally responsive prostate cancer. *Cancer Discovery*, 2:995-1003.
11. Ozkumur, E., Shah, A.M., Ciciliano, J.C., Emmink, B.L., **Miyamoto, D.T.**, Brachtel, E., Yu, M., Chen, P., Morgan, B., Trautwein, J., Kimura, A., Sengupta, S., Stott, S.L., Karabacak, N.M., Barber, T.A., Walsh, J.R., Smith, K., Spuhler, P., Sullivan, J., Lee, R., Ting, D.T., Luo, X., Shaw, A.T., Bardia, A., Sequist, L.V., Louis, D.N., Maheswaran, S., Kapur, R., Haber, D.A., Toner, M. (2013). Inertial Focusing for Positive and Negative Sorting of Rare Circulating Tumor Cells. *Science Translational Medicine,* 5:179ra47.
12. Lee, R.J., Saylor, P.J., Michaelson, M.D., Rothenberg, S.M., Smas, M.E., **Miyamoto, D.T.**, Gurski, C.A., Xie, W., Maheswaran, S., Haber, D.A., Goldin, J.G., Smith, M.R. (2013). A dose-ranging study of cabozantinib in men with castration-resistant prosate cancer and bone metastases. *Clinical Cancer Research*, 19(11):3088-94.
13. **Miyamoto, D.T.**, Viswanathan, A.N. (2013). Concurrent chemoradiation for vaginal cancer. *PLoS One*, 8(6): e65048. doi:10.1371/journal.pone.0065048.

Reviews and Book Chapters

1. **Miyamoto, D.T.** Probing the functions of kinesins in mitosis [dissertation]. Cambridge (MA): Harvard University; 2004.
2. **Miyamoto, D.T.**, Perlman, Z.E., Mitchison, T.J., and Shirasu-Hiza, M. (2003). Dynamics of the mitotic spindle – potential therapeutic targets. In: Meijer, L., Jezequel, A., and Roberge, M., editors. *Progress in Cell Cycle Research*, Volume 5. New York: Plenum Press; p. 349-60.
3. **Miyamoto, D.T.** and Harris, J.R. (2011). Molecular predictors of local tumor control in early-stage breast cancer. *Seminars in Radiation Oncology*, 21:35-42.

Abstracts (within the last 3 years)

1. Stott, S.L., Hsu, C.H., **Miyamoto, D.T.**, Rothenberg, S.M., Nagrath, S., Lee, R.J., Sequist, L.V., Maheswaran, S., Haber, D.A., Toner, M. (October, 2010). Isolation of circulating tumor cells from cancer patients using a microfluidic vortex generator. Biomedical Engineering Society 2010 Annual Meeting, Austin, TX. (Oral Presentation).
2. **Miyamoto, D.T.**, Tanaka, C.K., Viswanathan, A.K. (November, 2010). Concurrent chemoradiation improves survival in patients with vaginal cancer. American Society for Radiation Oncology 52nd Annual Meeting, San Diego, CA. (Oral Presentation).
3. Stott, S.L., Rothenberg, S.M., **Miyamoto, D.T.**, Lee, R.J., Sequist, L.V., Maheswaran, S., Haber, D.A., Toner, M. (October, 2011). Multi-parameter characterization of circulating tumor cells isolated from cancer patients using a microfluidic vortex generator. Biomedical Engineering Society 2011 Annual Meeting, Hartford, CT. (Oral Presentation).
4. Lee, R.J., Michaelson, M.D., Saylor, P.J., Gurski, C.A., Rothenberg, S.M., **Miyamoto, D.T.**, Maheswaran, S., Haber, D.A., Goldin, J.G., Smith, M.R. (June, 2012). Investigator-sponsored trial of efficacy and tolerability of cabozantinib (cabo) at lower dose: A dose-finding study in men with castration-resistant prostate cancer (CRPC) and bone metastases. 2012 ASCO Annual Meeting, Chicago, IL. (Poster Discussion Session).
5. **Miyamoto, D.T.,** Lee, R.J., Stott, S.L., Ting, D.T., Wittner, B.S., Ulman, M., Smas, M.E., Lord, J.B., Brannigan, B.W., Trautwein, J., Bander, N.H., Wu, C.L., Sequist, L.V., Smith, M.R., Ramaswamy, S., Toner, M., Maheswaran, S., Haber, D.A. (October, 2012). Androgen receptor signaling in circulating tumor cells as a marker of hormonally responsive prostate cancer. Prostate Cancer Foundation 19th Annual Scientific Retreat, Carlsbad, CA. (Poster Presentation).

D. Research Support

Ongoing Research Support

Dana Farber/Harvard Cancer Center — Miyamoto (PI) — 08/01/2011-07/31/2013
A. David Mazzone Career Development Award
Analysis of androgen receptor signaling in circulating tumor cells in prostate cancer.

Department of Defense — Miyamoto (PI) — 07/01/2012 – 06/30/2017
Physician Research Training Award, Prostate Cancer Research Program
Probing androgen receptor signaling in circulating tumor cells in prostate cancer.

NCI/MGH
Federal Share of the Proton Beam Program, Spiro Award — Miyamoto (PI) — 04/15/2012 – 04/14/2014
Evaluation of Multigene Expression Signatures as Predictors of Outcome After Radiation Therapy for Prostate Cancer

Pending Research Support

None

Completed Research Support

Howard Hughes Medical Institute Predoctoral Fellowship — Miyamoto (PI) — 07/01/2001-11/30/2004
Probing the functions of kinesins in mitosis.

NCI/MGH — Miyamoto (PI) — 07/01/2011-06/30/2012
Federal Share of the Proton Beam Program, Research Career Development Award
Molecular characterization of circulating tumor cells in prostate cancer.

Overlap

None

Published OnlineFirst on October 23, 2012; DOI:10.1158/2159-8290.CD-12-0222

RESEARCH BRIEF

Androgen Receptor Signaling in Circulating Tumor Cells as a Marker of Hormonally Responsive Prostate Cancer

David T. Miyamoto[1,3], Richard J. Lee[1,4], Shannon L. Stott[2,5], David T. Ting[1,4], Ben S. Wittner[1], Matthew Ulman[1], Malgorzata E. Smas[1], Jenna B. Lord[1], Brian W. Brannigan[1], Julie Trautwein[1], Neil H. Bander[7], Chin-Lee Wu[6], Lecia V. Sequist[1,4], Matthew R. Smith[1,4], Sridhar Ramaswamy[1,4], Mehmet Toner[2,5], Shyamala Maheswaran[1,5], and Daniel A. Haber[1,4,8]

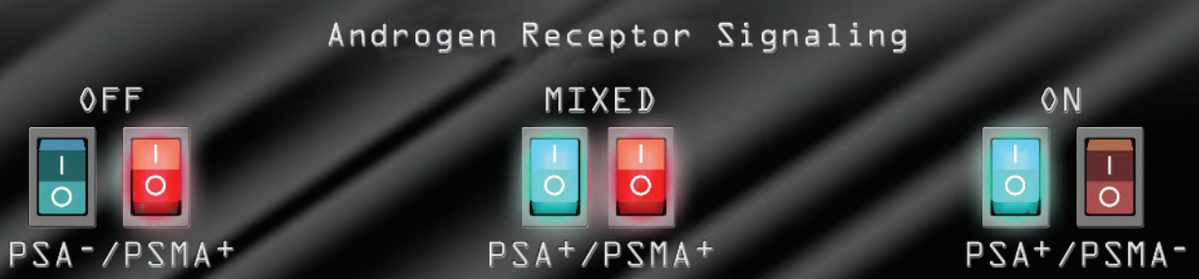

ABSTRACT

Androgen deprivation therapy (ADT) is initially effective in treating metastatic prostate cancer, and secondary hormonal therapies are being tested to suppress androgen receptor (AR) reactivation in castration-resistant prostate cancer (CRPC). Despite variable responses to AR pathway inhibitors in CRPC, there are no reliable biomarkers to guide their application. Here, we used microfluidic capture of circulating tumor cells (CTC) to measure AR signaling readouts before and after therapeutic interventions. Single-cell immunofluorescence analysis revealed predominantly "AR-on" CTC signatures in untreated patients, compared with heterogeneous ("AR-on, AR-off, and AR-mixed") CTC populations in patients with CRPC. Initiation of first-line ADT induced a profound switch from "AR-on" to "AR-off" CTCs, whereas secondary hormonal therapy in CRPC resulted in variable responses. Presence of "AR-mixed" CTCs and increasing "AR-on" cells despite treatment with abiraterone acetate were associated with an adverse treatment outcome. Measuring treatment-induced signaling responses within CTCs may help guide therapy in prostate cancer.

SIGNIFICANCE: Acquired resistance to first-line hormonal therapy in prostate cancer is heterogeneous in the extent of AR pathway reactivation. Measurement of pre- and posttreatment AR signaling within CTCs may help target such treatments to patients most likely to respond to second-line therapies. *Cancer Discov; 2(11); 1–9. ©2012 AACR.*

Authors' Affiliations: [1]Massachusetts General Hospital Cancer Center, [2]Center for Bioengineering in Medicine and Departments of [3]Radiation Oncology, [4]Medicine, [5]Surgery and [6]Pathology, Harvard Medical School, Charlestown, Massachusetts; [7]Weill Cornell Medical College, New York Presbyterian Hospital, New York, New York; and [8]Howard Hughes Medical Institute, Chevy Chase, Maryland

Note: Supplementary data for this article are available at Cancer Discovery Online (http://cancerdiscovery.aacrjournals.org/).

D.T. Miyamoto, R.J. Lee, and S.L. Stott contributed equally to this work.

Corresponding Authors: Daniel Haber, Cancer Center, Massachusetts General Hospital, Building 149, 13th Street, Charlestown, MA 02129. Phone: 617-726-7805; Fax: 617-724-6919; E-mail: Haber@helix.mgh.harvard.edu; and Shyamala Maheswaran, E-mail: maheswaran@helix.mgh.harvard.edu.

doi: 10.1158/2159-8290.CD-12-0222

Published OnlineFirst on October 23, 2012; DOI:10.1158/2159-8290.CD-12-0222

INTRODUCTION

Prostate cancer is highly dependent upon androgen receptor (AR) signaling for cell proliferation and survival. Androgen deprivation therapy (ADT) results in high rates of initial response in most patients with metastatic prostate cancer. However, disease progression is invariably observed with tumor cells resuming proliferation despite continued treatment (termed castration-resistant prostate cancer or CRPC; ref. 1). The propensity of metastatic prostate cancer to spread to bone has limited repeated sampling of tumor deposits that have acquired castration resistance, but insights into resistance mechanisms have emerged through bone marrow biopsy and autopsy studies, as well as mouse modeling experiments (2). The concept that CRPC results from reactivation of AR signaling despite low levels of serum testosterone is consistent with a frequently observed rise in serum prostate-specific antigen (PSA), an androgen-responsive gene product secreted into blood by prostate cancer cells (1, 2). Potential mechanisms by which AR reactivation occurs in CRPC include variable levels of *AR* gene amplification (~30% of cases), activating *AR* mutations, alternative mRNA splicing (~10%), increased expression or activation of AR transcriptional coactivators, activation of modulatory kinase pathways [e.g., Ras, phosphoinositide-3 kinase (PI3K)], tyrosine phosphorylation of AR, and increased intratumoral androgen synthesis; (see ref. 2 for review). The functional significance of reactivated AR signaling in CRPC has been inferred from mouse xenograft models of prostate cancer, in which even modest increases in *AR* gene expression cause tumors to become resistant to castration (3).

The concept of AR reactivation in CRPC has become therapeutically relevant with the development of potent novel inhibitors of AR signaling (4, 5). The demonstration that abiraterone acetate, a CYP17A1 inhibitor that potently suppresses adrenal and intratumoral steroid biosynthesis, increases overall survival in men with metastatic CRPC who have previously received chemotherapy lends support to the rationale of suppressing AR reactivation in CRPC (5). Notably, there is a wide variation in patient response to abiraterone acetate as measured by serum PSA (5), and there is an unmet need for reliable biomarkers that can predict treatment response to abiraterone acetate and other potent inhibitors of AR signaling under development. Taking advantage of recent technological advances in the capture, imaging, and molecular characterization of rare circulating tumor cells (CTC) shed into blood from otherwise poorly accessible metastatic tumor deposits (6, 7), we established a noninvasive "real time" measure of intratumoral AR signaling before and after initial- or second-line hormonal therapy in patients with metastatic prostate cancer.

RESULTS

Single-Cell Measurement of AR Signaling Parameters in Prostate CTCs

To measure the status of AR signaling within individual cells, we established a quantitative immunofluorescence assay based on the expression of AR-regulated genes. We reasoned that such a readout would be independent of mechanisms of AR reactivation in CRPC (e.g., *AR* amplification or mutation, ligand overexpression, or AR cofactor misregulation) and would therefore provide a clear measure of whether the AR pathway has been reactivated during the acquisition of resistance to ADT. To identify optimal downstream readouts of AR signaling, we subjected a prostate cancer cell line (LNCaP) to androgen deprivation or stimulation, and used digital gene expression profiling to identify transcripts that are differentially regulated in response to changes in AR signaling (Supplementary Fig. S1). Among candidate gene products that are prostate cancer–specific and for which reliable antibodies are available, we selected PSA (*KLK3*) and prostate-specific membrane antigen (PSMA; *FOLH1*) as most consistently upregulated following AR activation and AR suppression, respectively (Fig. 1A and B; Supplementary Fig. S1A and S1B). Selection of PSMA as a marker of AR suppression was also recently described by Evans and colleagues while this work was in progress (8).

Our assay for quantitative measurement of signal intensity profiles for cells stained with antibodies against PSA and PSMA was developed using a model cell system (LNCaP). Treatment of androgen-starved LNCaP cells with the androgen R1881 and measurement of immunofluorescence signals using an automated fluorescence microscopy scanning platform revealed time-dependent progression from an initial "AR-off" ($PSA^-/PSMA^+$) to an intermediate "AR-mixed" ($PSA^+/PSMA^+$) phenotype, and finally to an "AR-on" ($PSA^+/PSMA^-$) pattern (Fig. 1C; Supplementary Fig. S2A). The reverse progression was observed upon treatment with the AR inhibitor bicalutamide (Fig. 1D; Supplementary Fig. S2B). Similar results were observed using VCaP cells, another androgen-responsive prostate cancer cell line (Supplementary Fig. S3).

For isolation of CTCs, we made use of our recently developed "second-generation" microfluidic chip, in which herringbone (HB) grooves in the ceiling of the channel create anisotropic flow conditions, generating microvortices that direct cells toward the anti–epithelial cell adhesion molecule (EpCAM) antibody–coated walls of the device (^{HB}CTC-Chip; ref. 7). ^{HB}CTC-Chip parameters for single-cell AR signaling analysis were first established by modeling LNCaP cells treated with R1881 or bicalutamide, spiked into control blood specimens, captured on the ^{HB}CTC-Chip, and stained with antibodies against PSA and PSMA (AR signaling) along with anti-CD45 (to exclude contaminating leukocytes) and 4′, 6-diamidino-2-phenylindole (DAPI; for nuclear morphology; Supplementary Fig. S4A and S4B). To achieve multiparameter single-cell analysis of AR activity, an automated fluorescence microscopy scanning platform was adapted to distinctly and specifically measure 4 fluorescent emission spectra simultaneously. We carefully selected the choice of secondary fluorophores and optical band pass filters to avoid "cross-talk" between the multiple fluorescent signals that are closely located on the electromagnetic spectrum while maximizing signal intensity (see Methods). The 4-color immunofluorescence imaging parameters established using LNCaP cells were then applied to accurately enumerate patient-derived CTCs (Fig. 2a). To minimize the risk of counting false-positive events as CTCs, we adopted a previously reported strategy (6), calibrating threshold signal intensity and setting a cut-off value for detection of CTCs based on the number of positive events detected in healthy donor samples. Using the newly optimized 4-color

Published OnlineFirst on October 23, 2012; DOI:10.1158/2159-8290.CD-12-0222

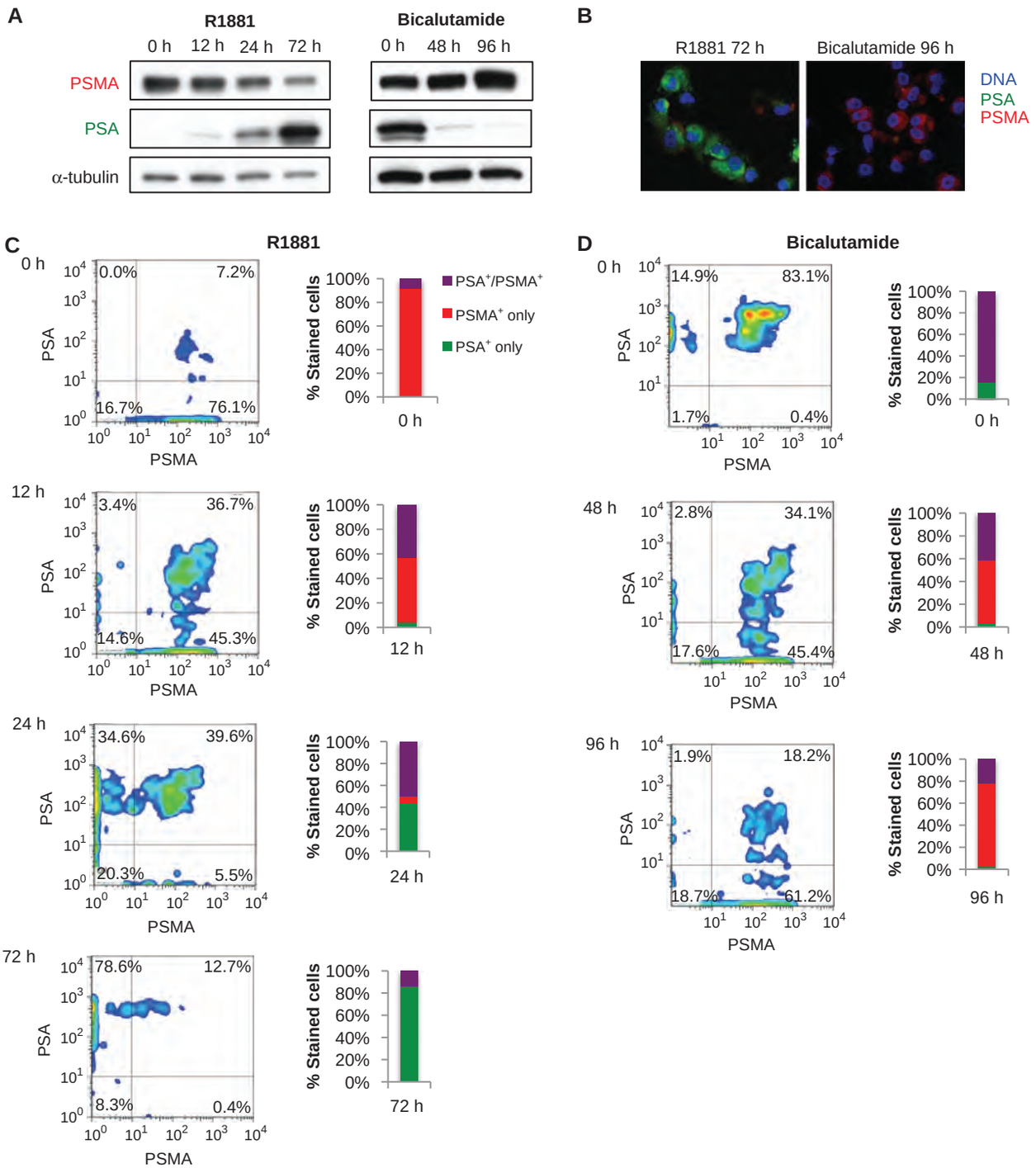

Figure 1 . Multiparameter single-cell immunofluorescence assay to measure changes in AR activity in cultured prostate cancer cells. **A,** Western blot analysis for PSA, PSMA, and α-tubulin in LNCaP cells treated with 1 nmol/L R1881 after being cultured under androgen-deprived conditions (left), or treated with 10 mol/L bicalutamide after being cultured under standard conditions (right). **B,** merged immunofluorescence images of LNCaP cells dual stained with antibodies against PSA (green) and PSMA (red) after treatment with 1 nmol/L R1881 or 10 mol/L bicalutamide. **C,** pseudocolor density plots of multiparameter immunofluorescence profiles of LNCaP cells treated with 1 nmol/L R1881, imaged using an automated fluorescence microscopy scanning system. *x*- and *y*-axes represent "area-pixel" single-cell signal intensity measurements for PSMA and PSA, respectively. The total fraction of $PSA^+/PSMA^-$ (AR-on), $PSA^-/PSMA^+$ (AR-off), and $PSA^+/PSMA^+$ (AR-mixed) cells is shown in the bar graph. **D,** comparable analysis for LNCaP cells treated with 10 mol/L bicalutamide after being cultured under standard conditions.

Published OnlineFirst on October 23, 2012; DOI:10.1158/2159-8290.CD-12-0222

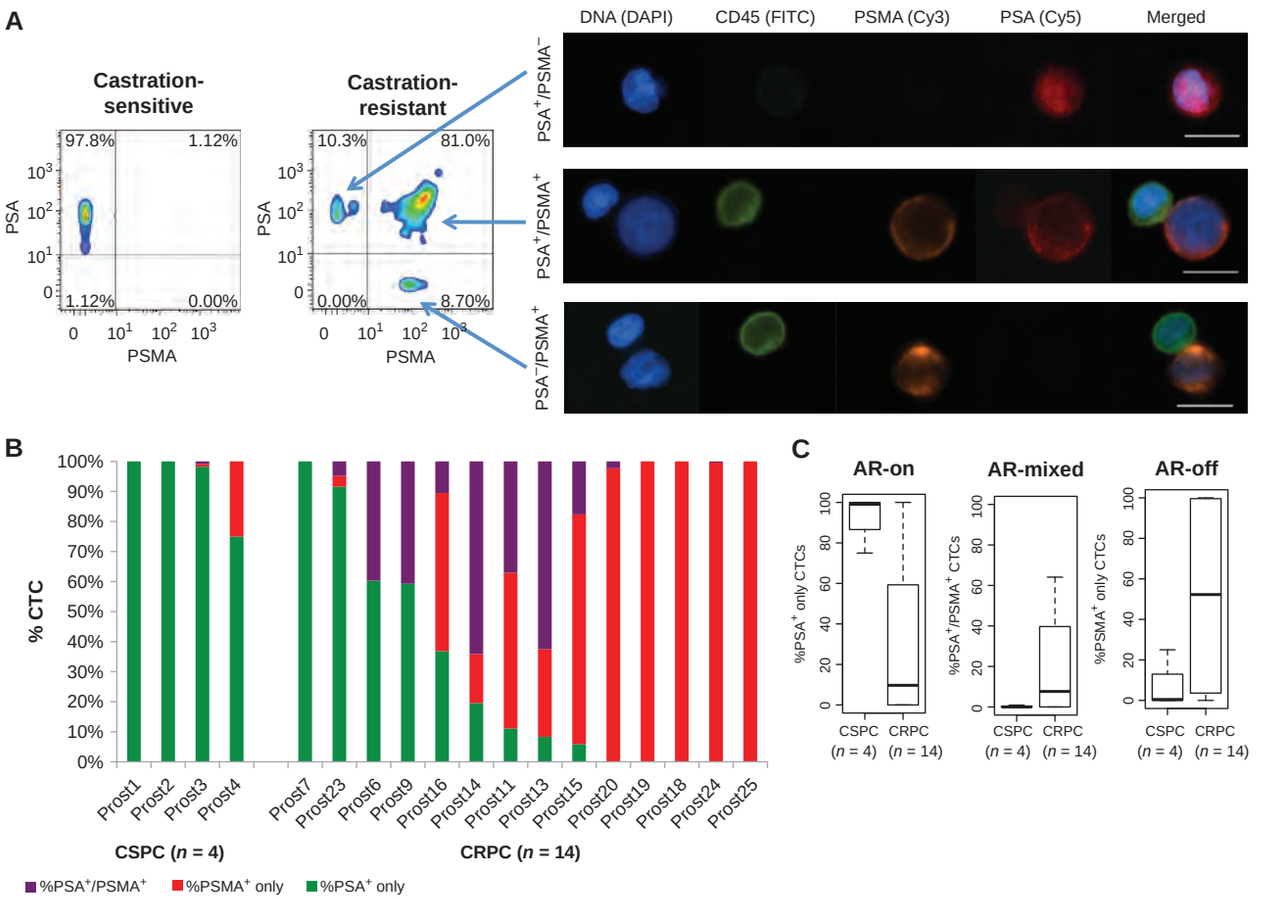

Figure 2 . Single-cell measurements of AR signaling identify predominantly "AR-on" CTCs in castration-sensitive prostate cancer (CSPC) versus heterogeneous signatures in CRPC. **A,** pseudocolor density plots of multiparameter immunofluorescence profiles of CTCs from patient with CSPC (left) and CRPC (right). *x*- and *y*-axes represent "area-pixel" single-cell signal intensity measurements for PSMA and PSA, respectively. Representative images are depicted of an "AR-on" ($PSA^+/PSMA^-$) CTC (top row on right), an "AR-mixed" ($PSA^+/PSMA^+$) CTC (middle row), and an "AR-off" ($PSA^-/PSMA^+$) CTC (bottom row), with CD45 (FITC), PSMA (Cy3), and PSA (Cy5). Contaminating $CD45^+$ leukocytes are depicted for comparison in the middle and bottom rows. Scale bars, 10 m. **B,** bar graphs showing proportional distribution of AR signaling phenotypes in CTCs from patients with CSPC or CRPC before initiation of therapy. Patient samples are ordered according to relative percentage of "AR-on" PSA^+ only CTCs. **C,** box plots showing the relative proportions of AR signaling phenotypes in CTCs from patients with CSPC compared with CRPC before initiation of therapy ($P = 0.012$ for $PSA^+/PSMA^-$; $P = 0.071$ for $PSA^+/PSMA^+$; $P = 0.076$ for $PSA^-/PSMA^+$).

immunofluorescence imaging parameters, we established a threshold value for positive CTC detection of more than 4 PSA^+ or $PSMA^+/CD45^-$ cells/mL, which was higher than any count noted in any healthy donor sample (Supplementary Fig. S5). The expansion of our CTC characterization to include 4-color staining in a high-throughput manner required the use of new organic fluorophores, narrow band fluorescent filter cubes, and a new automated imaging platform (see Methods). The result was a more specific assay with less background signal in our healthy donors compared with our previous papers (6, 7). We tested the validity of this threshold cut-off value in a separate cohort of age-matched male patients with no known diagnosis of cancer. Using this threshold, CTCs were not detectable in any patients without a diagnosis of prostate cancer ($n = 0/21$; Supplementary Fig. S5). In contrast, subsequent analysis of pretreatment blood samples from patients with metastatic prostate cancer revealed detectable CTCs above the predetermined threshold cut-off in 72% of patients ($n = 18/25$; Supplementary Fig. S5 and Supplementary Table S1).

Active AR Signaling in CTCs from Untreated Patients with Metastatic Prostate Cancer

Having standardized CTC detection using 4-color imaging criteria, we applied the PSA/PSMA dual immunophenotyping assay to patients with newly diagnosed metastatic prostate cancer. CTCs were detectable in 4 of 5 (80%) patients with newly diagnosed metastatic prostate cancer before the initiation of ADT. AR activity was predominantly positive among the patients with detectable CTCs, with the vast majority (median 99.1%; range, 75%–100%) of isolated CTCs from each patient showing the "AR-on" ($PSA^+/PSMA^-$) phenotype (Figs. 2B and C; Supplementary Table S2). The initiation of ADT in treatment-naïve patients with metastatic prostate cancer with detectable CTCs resulted in transformation of the majority of CTCs from the "AR-on" to the "AR-off" phenotype within 1 month, followed by the complete disappearance of CTCs by 3 months after initiation of therapy (Fig. 3A–C; Supplementary Table S2).

Published OnlineFirst on October 23, 2012; DOI:10.1158/2159-8290.CD-12-0222

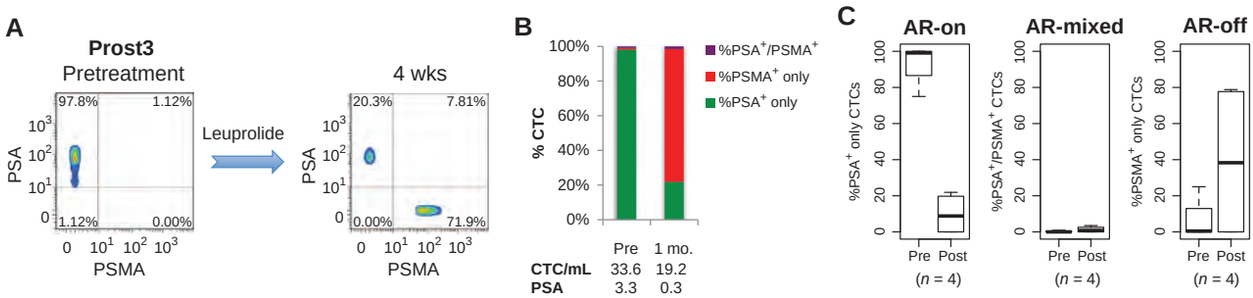

Figure 3 . ADT-induced AR signaling changes in CTCs from patients with castration-sensitive metastatic prostate cancer. **A,** pseudocolor density plots of multiparameter immunofluorescence AR signaling profiles of CTCs in a patient (Prost3) with CSPC before and after ADT with leuprolide showing transformation of CTCs from the "AR-on" ($PSA^+/PSMA^-$) phenotype to the "AR-off" ($PSA^-/PSMA^+$) phenotype. **B,** bar graphs showing proportional distribution of AR signaling phenotypes in CTCs from this patient before and after ADT. Corresponding CTC numbers and serum PSA levels are shown for pretreatment (pre) and after therapy. **C,** box plots showing composite data for relative proportions of AR signaling phenotypes in CTCs from patients with CSPC ($n = 4$) pretreatment and after 4 weeks of ADT ($P = 0.028$ for $PSA^+/PSMA^-$; $P = 0.41$ for $PSA^+/PSMA^+$; $P = 0.64$ for $PSA^-/PSMA^+$).

Heterogeneous AR Signaling in CTCs from Patients with CRPC

In marked contrast, patients with CRPC with detectable CTCs pretreatment (n = 14/20; 70%) displayed both intrapatient and interpatient heterogeneity in CTC AR activity (Fig. 2; Supplementary Table S2). Most remarkable was the abundance within each patient of CTCs with the "AR-off" ($PSA^-/PSMA^+$) signature (median 51.9%), as well as CTCs with an "AR-mixed" ($PSA^+/PSMA^+$) phenotype (median 17.6%). Despite the expected reactivation of AR signaling in CRPC, only a relatively small fraction of CTCs in these patients had the "AR-on" ($PSA^+/PSMA^-$) phenotype (median 11.1%). In contrast to the consistent treatment-induced changes in AR signaling patterns seen within CTCs of patients with castration-sensitive prostate cancer (CSPC), second-line hormonal treatment in patients with CRPC had varying effects on CTC numbers and AR phenotypes (Fig. 4; Supplementary Tables S1 and S2). This included patients treated with the relatively weak hormonal agents ketoconazole ($n = 1$) and bicalutamide (n = 2), as well as the potent CYP17A1 inhibitor abiraterone acetate (n = 17; Supplemental Table S2). Four of 17 (24%) patients with CRPC treated with abiraterone acetate had a 50% or more decline in the percentage of "AR-on" CTCs within 2 to 5 weeks of therapy, suggesting that the reduction in systemic androgen levels may have suppressed a subset of metastatic tumor cells with reactivated AR signaling (Fig. 4A–C; Supplementary Tables S1 and S2). In contrast, 2 of 17 (12%) patients with CRPC had a 2-fold or more increase in the percentage of "AR-on" CTCs within the first 2 to 5 weeks of therapy with abiraterone acetate, suggesting increased AR signaling despite therapy (Fig. 4D–F; Supplementary Tables S1 and S2). Eleven of 17 (65%) patients with CRPC had a stable percentage of "AR-on" CTCs after therapy. Analysis of baseline CTC AR signaling before the initiation of abiraterone acetate therapy suggested that the presence of a more than 10% component of "AR-mixed" CTCs was associated with decreased overall survival (log-rank $P < 0.05$; Fig. 4G). In addition, an increase in the percentage of "AR-on" CTCs despite abiraterone acetate therapy was correlated with decreased overall survival (Supplementary Fig. S6).

DISCUSSION

Cancer cells circulating in the peripheral blood provide a uniquely accessible source of tumor-derived material for molecular analyses. In metastatic prostate cancer, which primarily spreads to bone, the inability to noninvasively sample metastatic lesions has limited the ability to individualize second-line therapies according to the mechanism of drug resistance. Thus, while potent new inhibitors of the AR pathway are under active development, their clinical deployment still remains empiric. Given the interpatient variation in outcome, there is an unmet clinical need for biomarkers that may enable prediction of treatment response for individual patients. Here, we show that the activity of the AR pathway may be monitored in CTCs. Although the trends we observe need confirmation in subsequent analysis with additional patients, our results support the relevance of CTCs as dynamic tumor-derived biomarkers, reflecting "real time" effects of cancer drugs on their therapeutic targets, and the potential of CTC signaling analysis to identify the early emergence of resistance to therapy.

Although CTC enumeration using immunomagnetic bead capture has previously been shown to be a potential prognostic biomarker in patients with metastatic prostate cancer (9), enumeration alone does not yield direct insight into the effects of drugs on their molecular targets and may simply reflect relative tumor burden or leakiness of tumor-associated vasculature. In contrast, interrogation of the activity of specific signaling pathways within CTCs may reveal whether targeted therapies are effectively hitting their target *in vivo*, thus providing information that may be useful in guiding therapeutic decisions. Reverse transcription–PCR of transcripts from CTC-enriched cell populations may provide an alternative method for detecting CTCs (10), with the potential for measuring changes in relevant transcriptional output in CTCs. However, the need for quantitative analysis of signal within the heterogeneous cell populations, as documented here, supports the importance of single-cell measurements based on CTC imaging.

Because PSMA is a cell surface protein, it has been used as an alternative to EpCAM for capture of CTCs from patients with prostate cancer (11). Although more specific to prostate

Published OnlineFirst on October 23, 2012; DOI:10.1158/2159-8290.CD-12-0222

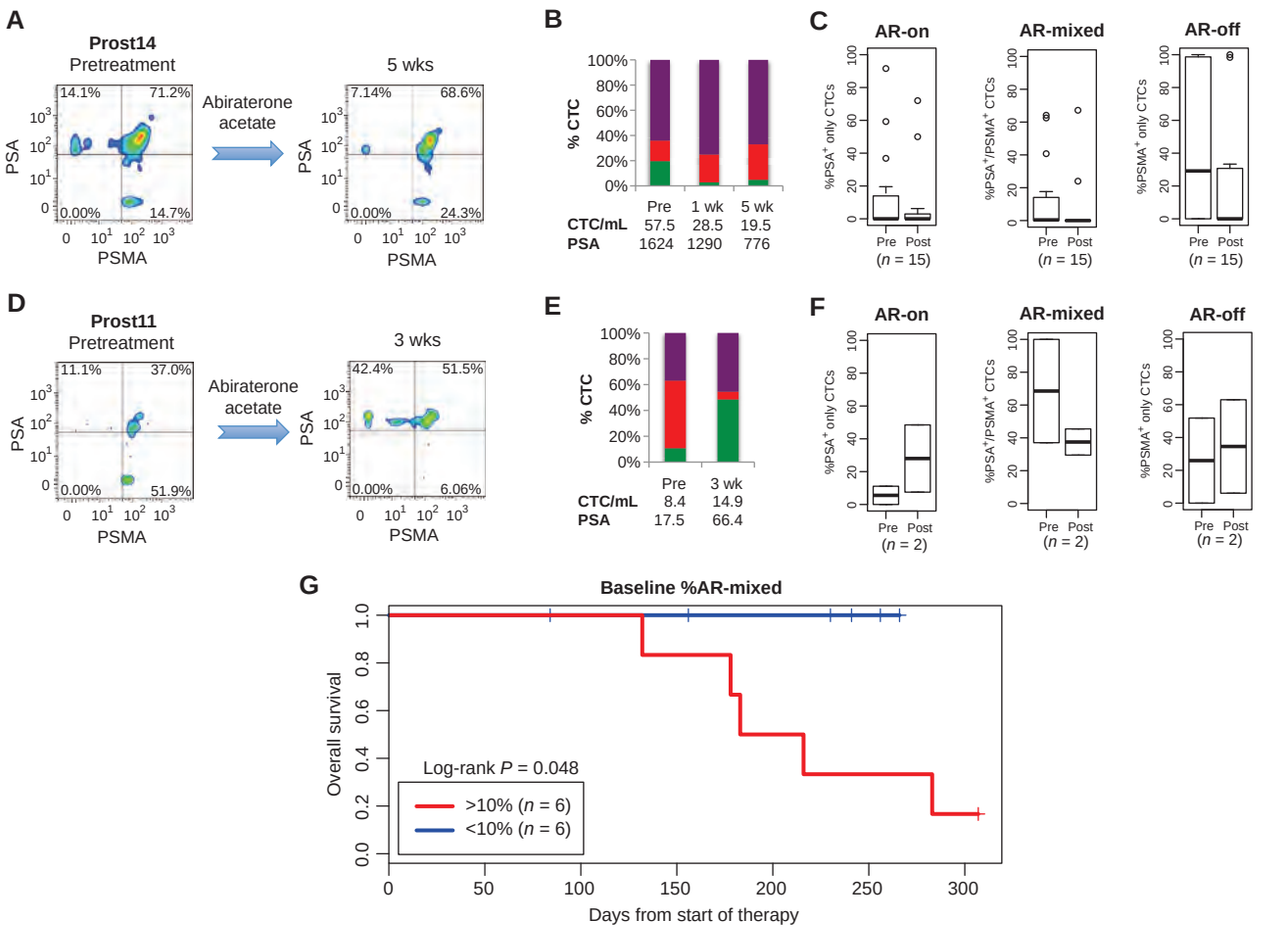

Figure 4 . AR signaling in CTCs from CRPC patients treated with abiraterone acetate. **A,** pseudocolor density plots of multiparameter immunofluorescence AR signaling profiles of CTCs in a patient (Prost14) with CRPC, showing a decrease in the proportion of PSA$^+$/PSMA$^-$ "AR-on" CTCs after the initiation of abiraterone acetate. **B,** Bar graphs depicting the results for this patient at serial time points following treatment. Corresponding CTC numbers and serum PSA levels are shown for pretreatment (pre) and at weeks following therapy. **C,** box plots showing composite data for relative proportions of AR signaling phenotypes in CTCs from patients that exhibit stable or declining proportion of "AR-on" CTCs after initiation of therapy ($P = 0.56$ for PSA$^+$ only; $P = 0.12$ for PSA$^+$/PSMA$^+$; $P = 0.14$ for PSMA$^+$ only). **D,** increase in the proportion of PSA$^+$/PSMA$^-$ "AR-on" CTCs observed in a patient (Prost11) with CRPC after treatment with abiraterone acetate. **E,** bar graphs depicting the results for this patient. **F,** box plots showing composite data for relative proportions of AR signaling phenotypes in CTCs from patients that exhibit an increasing proportion of "AR-on" CTCs after initiation of therapy ($P = 0.67$ for PSA$^+$ only; $P = 0.67$ for PSA$^+$/PSMA$^+$; $P = 0.67$ for PSMA$^+$ only). **G,** Kaplan–Meier curves for overall survival in patients with CRPC treated with abiraterone acetate, according to baseline percentage of more than 10% "AR-mixed" CTCs (red) versus less than 10% "AR-mixed" CTCs [(blue) log-rank $P = 0.048$].

cancer, PSMA-based capture may miss the "AR-on" subsets of CTCs, whose phenotype is primarily PSA$^+$/PSMA$^-$, and which may be important in defining response to hormonal therapies. As such, anti-EpCAM antibody-mediated capture followed by immunophenotyping for PSA versus PSMA expression allows for broad capture of CTCs, followed by characterization of their AR signaling status. Critical for this approach is the optimization of 4-color immunofluorescence staining and imaging parameters, maximizing immunofluorescence signals, while minimizing cross-talk between channels for detection of PSA, PSMA, CD45, and nuclear signals, using a standardized semi-automated microscopy platform. Full automation of this assay will be required for its broad application in the context of clinical trials of novel hormonal agents in CRPC.

Although our study was designed as a "proof-of-concept" for a diagnostic approach, it also provides significant insight into the evolution of initially responsive prostate cancer into castration-resistant disease. We found that profound differences underlie the dramatic response of previously untreated, castration-sensitive disease to ADT, compared with the relatively limited effectiveness of even potent second-line hormonal agents in castration-resistant disease. CSPC is marked by the presence of predominant and strong "AR-on" CTC signals, with rapid switching to "AR-off" upon androgen withdrawal, preceding the disappearance of CTCs from the circulation. In contrast, CRPC is marked by striking heterogeneity among tumor cells from individual patients as well as between different patients with similar clinical histories. Few "AR-on" cells are observed, and instead there is an abundance of both "AR-off" and "AR-mixed" CTCs. Together, these suggest that pathways other than AR signaling contribute to disease progression in CRPC, and that the AR reactivation that

Published OnlineFirst on October 23, 2012; DOI:10.1158/2159-8290.CD-12-0222

does occur may be qualitatively altered despite the known overexpression of AR itself. Indeed, reactivation of AR signaling in CRPC does not seem to be as complete as previously suspected, and even potent AR suppression in this setting may be insufficient by itself to mediate dramatic tumor responses. Rising serum PSA levels in patients with CRPC have been taken as evidence of strong AR reactivation and potentially renewed susceptibility to hormonal manipulation. However, these serum measurements reflect total tumor burden, which may be considerable, whereas single-cell CTC analysis suggests that within individual tumor cells, AR signaling is not fully reactivated.

Although AR reactivation is the dominant model to explain acquisition of resistance to androgen withdrawal, the limited human data available are consistent with our observations of an attenuated AR phenotype in CRPC. For instance, gene expression studies of bone metastases have shown increased AR mRNA levels in CRPC (12), and bone marrow biopsy studies (13) as well as CTC analyses (14) have shown nuclear AR localization in resistant disease. However, expression levels of androgen-activated genes seem to be reduced by 2- to 3-fold in CRPC, compared with primary untreated prostate cancer (12, 15). The most common acquired genetic alteration affecting *AR*, a median 1.6- to 5-fold gene amplification seen in approximately 30% of cases (16, 17), may not be sufficient to fully overcome the effects of ligand withdrawal and reestablish full AR-driven tumor cell proliferation. Indeed, a recent analysis of gene promoters targeted by AR in cells that are sensitive to androgen withdrawal versus cells with acquired resistance showed a qualitatively distinct subset of AR-activated genes (18, 19). In our study, the complexity of AR signaling pathways in CRPC may be reflected by the presence of "AR-mixed" CTCs having simultaneous expression of androgen-induced and androgen-suppressed markers that was associated with decreased overall survival. Thus, expression analysis of AR target genes within CTCs may provide functionally relevant measures of aberrant AR activity.

In addition to altered AR signaling, AR-independent pathways, including PIK3CA-dependent signaling, have also been implicated in CRPC and may cooperate with partial AR reactivation in mediating disease progression in prostate cancer (20). Recent studies in mouse models of CRPC have suggested improved responses to combined AR and mTOR pathway inhibition (20). Given the potentially complex and heterogeneous mechanisms underlying CRPC, it is not surprising that treatment with the potent CYP-17A1 inhibitor abiraterone acetate alone has a varied effect on the number and composition of CTCs. Some patients with CRPC who did have measureable "AR-on" CTCs showed more than 50% decline in the percentage of this CTC subset within 2 to 5 weeks of abiraterone acetate therapy (4 of 17 patients; 24%). Given the mechanism of drug action, these cases may be enriched for patients in whom intratumoral or adrenal gland synthesis of androgens plays a major role in the development of castration resistance. In contrast, tumors driven by ligand-independent *AR* gene activation would not be expected to show any suppression in "AR-on" CTC numbers. Indeed, a rising fraction of "AR-on" CTCs despite continued abiraterone acetate therapy was associated with a poor outcome, defined as decreased overall survival. In these patients, ligand-independent AR activity may become a driver of tumor cell proliferation, leading to therapeutic failure. Potential mechanisms for the development of resistance to abiraterone acetate in CRPC are the subject of intense investigation (21). Further studies linking such mechanistic insights with the application of novel therapies targeting the relevant pathways may provide critical guidance in molecularly targeted therapy for CRPC.

In summary, in this exploratory study, we show that PSA/PSMA-based AR signaling assay in CTCs may enable real-time quantitative monitoring of intratumoral AR signaling and its potential contribution to disease progression within an individual patient. Although this assay has potential as a promising biomarker, it requires validation in larger prospective studies of patients with prostate cancer undergoing second-line hormonal therapy. While this work was in progress, positron emission tomography imaging using radiolabeled antibodies against PSMA and PSA were reported as biomarkers of AR signaling in prostate cancer mouse xenografts treated with the investigational AR inhibitor MDV 3100 (8, 22). If successful in human tumor imaging, radioisotope scanning for AR activity may complement single-cell CTC assays in providing ongoing monitoring for second-line hormonal agents in CRPC. Such individualization of second-line treatments in metastatic prostate cancer will be essential for therapeutic success, given the evident tumor cell heterogeneity that accompanies the emergence of resistance to initial androgen deprivation.

METHODS

Patients and Clinical Specimens

Patients with metastatic prostate cancer receiving treatment at the Massachusetts General Hospital (Boston, MA) were recruited according to an institutional review board (IRB)–approved protocol. Eligibility criteria included a histologic diagnosis of prostate adenocarcinoma and radiographic evidence of metastatic disease. For the CSPC cohort, recipients of prior hormonal therapy were excluded. Patients in the CRPC cohort required disease progression on ADT according to Prostate Cancer Working Group criteria (23), and may have received other therapies. A total of 25 patients donated 10 to 20 mL of blood on one or more occasions for CTC analysis. In addition, 21 male patients with no known diagnosis of cancer were recruited as controls using a separate IRB-approved protocol.

Cell Lines

LNCaP and VCaP cells were obtained from American Type Culture Collection after authentication by short tandem repeat profiling, and maintained as recommended. For generation of the AR signature, cells were cultured for 3 days in medium containing 10% charcoal-stripped FBS (Invitrogen) and treated with R1881 (Perkin-Elmer), bicalutamide (Sigma), or dimethyl sulfoxide (DMSO) as a vehicle control.

Immunofluorescence Staining and Automated Fluorescence Microscopy

Cells were captured on the ^{HB}CTC-chip as described (7), fixed and permeabilized as described (7), and stained with antibodies against PSA (rabbit polyclonal; DAKO), PSMA (J591 mouse monoclonal IgG1; N.H. Bander), and CD45 (mouse monoclonal IgG2a; Abcam), followed by appropriately matched secondary antibodies conjugated with DyLight 649 (Jackson ImmunoResearch), Alexa Fluor 555 (Invitrogen), and Alexa Fluor 488 (Invitrogen). Nuclei were stained with DAPI. An automated fluorescence microscopy scanning system (BioView)

comprehensively imaged ^{HB}CTC-chips under ×10 magnification in seven *z*-planes in 4 colors at predetermined optimized exposure times, using modified Magnetron sputter-coated filter sets for the Cy3 and Cy5 spectra (Chroma; see Supplementary Methods for details). Potential CTCs were automatically classified using a previously described algorithm (6), followed by manual validation by a blinded human reviewer. High-resolution immunofluorescence images were obtained using an upright fluorescence microscope (Eclipse 90i, Nikon) under ×60 magnification.

Quantitative Single-Cell Immunofluorescence Analysis

Quantitative fluorescence intensity data for emission spectra (DAPI, FITC, Cy3, and Cy5) were obtained for each single cell as "Area pixels" measurements using image analysis software (Bioview). Data files were converted to CSV format and to FCS format (TextToFCS version 1.2.1; ref. 24) and analyzed using FlowJo version 7.6. Pseudocolor density plots were gated to display events that are CD45$^-$. Bar graphs were generated using Microsoft Excel reflecting proportions of PSA$^+$/PSMA$^-$/CD45$^-$, PSA$^+$/PSMA$^+$/CD45$^-$, and PSA$^-$/PSMA$^+$/CD45$^-$ CTCs tabulated after manual validation. Normalized counts (CTC/mL) were calculated by dividing the total CTC count by the total blood volume processed. A signal intensity threshold of detection based on healthy donors was determined to be 4 CTC/mL (Supplementary Fig. S5). Normalized counts below this threshold were considered as false-positive events and not included in the final analyses. In cases where normalized CTC counts were below the limit of reliable detection, percentage distributions of AR signaling phenotypes were not calculated (Supplementary Table S1).

Statistical Analysis

AR activity and the proportion of CTC phenotypes between samples were compared using the Wilcoxon rank-sum test. Overall survival was defined as the interval between the start of therapy and the date of death or censor. Serum PSA response was defined as a maximal decline of 50% or more in serum PSA (23). Survival curves were generated using the Kaplan–Meier method and compared using the log-rank test. Two-sided P values <0.05 were considered statistically significant. Statistical analyses were conducted using R, version 2.12.0.

Disclosure of Potential Conflicts of Interest

N.H. Bander has ownership interest (including patents) and is a consultant/advisory board member in BZL Biologics, Inc. No potential conflicts of interest were disclosed by the other authors.

Authors' Contributions

Conception and design: D.T. Miyamoto, R.J. Lee, S.L. Stott, M.R. Smith, M. Toner, S. Maheswaran, D.A. Haber

Development of methodology: D.T. Miyamoto, R.J. Lee, S.L. Stott, C.-L. Wu, M. Toner, S. Maheswaran, D.A. Haber

Acquisition of data (provided animals, acquired and managed patients, provided facilities, etc.): D.T. Miyamoto, R.J. Lee, D.T. Ting, M. Ulman, M.E. Smas, J.B. Lord, B.W. Brannigan, J. Trautwein, C.-L. Wu, L.V. Sequist, M.R. Smith

Analysis and interpretation of data (e.g., statistical analysis, biostatistics, computational analysis): D.T. Miyamoto, R.J. Lee, S.L. Stott, B.S. Wittner, M. Ulman, M.E. Smas, J.B. Lord, B.W. Brannigan, S. Ramaswamy, S. Maheswaran, D.A. Haber

Writing, review, and/or revision of the manuscript: D.T. Miyamoto, R.J. Lee, S.L. Stott, N.H. Bander, C.-L. Wu, L.V. Sequist, M.R. Smith, M. Toner, S. Maheswaran, D.A. Haber

Administrative, technical, or material support (i.e., reporting or organizing data, constructing databases): D.T. Miyamoto, S.L. Stott, D.T. Ting, N.H. Bander

Study supervision: R.J. Lee, L.V. Sequist, S. Ramaswamy, M. Toner, S. Maheswaran, D.A. Haber

Acknowledgments

The authors thank J. Walsh, F. Floyd, G. Korir, C. Koris, and L. Libby for technical support.

In memory of Charles Evans and in recognition of philanthropic support for prostate cancer research from the Evans Foundation, we propose that this CTC-based test be called the Evans Assay.

Grant Support

This work was supported by a Challenge Grant from the Evans Foundation and the Prostate Cancer Foundation (PCF); a Stand Up To Cancer Dream Team Translational Cancer Research Grant, a Program of the Entertainment Industry Foundation (SU2C-AACR-DT0309, to D.A. Haber, M. Toner, and S. Maheswaran); T.J. Martell Foundation (to D.A. Haber); Starr Cancer Consortium (to D.A. Haber); the Susan G. Komen for the Cure KG090412 (S. Maheswaran); NIH-NIBIB-5R01EB008047 (to M. Toner and D.A. Haber); NCI-CA129933 (to D.A. Haber); the NCI-MGH Federal Share Program (to S. Maheswaran); NCI-C06-CA-059267 (to D.T. Miyamoto); NIH-5K12CA87723-09 (to D.T. Ting); Department of Defense Physician Research Training Awards (to D.T. Miyamoto and R.J. Lee); Mazzone-DF/HCC Career Development Award (to D.T. Miyamoto); Conquer Cancer Foundation Career Development Award and PCF Young Investigator Award (to R.J. Lee); American Cancer Society (to S.L. Stott); and Howard Hughes Medical Institute (to D.A. Haber).

Received May 15, 2012; revised August 22, 2012; accepted August 22, 2012; published OnlineFirst October 23, 2012.

REFERENCES

1. Scher HI, Sawyers CL. Biology of progressive, castration-resistant prostate cancer: directed therapies targeting the androgen-receptor signaling axis. J Clin Oncol 2005;23:8253–61.
2. Yuan X, Balk SP. Mechanisms mediating androgen receptor reactivation after castration. Urol Oncol 2009;27:36–41.
3. Chen CD, Welsbie DS, Tran C, Baek SH, Chen R, Vessella R, et al. Molecular determinants of resistance to antiandrogen therapy. Nat Med 2004;10:33–9.
4. Tran C, Ouk S, Clegg NJ, Chen Y, Watson PA, Arora V, et al. Development of a second-generation antiandrogen for treatment of advanced prostate cancer. Science 2009;324:787–90.
5. de Bono JS, Logothetis CJ, Molina A, Fizazi K, North S, Chu L, et al. Abiraterone and increased survival in metastatic prostate cancer. N Engl J Med 2011;364:1995–2005.
6. Stott SL, Lee RJ, Nagrath S, Yu M, Miyamoto DT, Ulkus L, et al. Isolation and characterization of circulating tumor cells from patients with localized and metastatic prostate cancer. Sci Transl Med 2010;2: 25ra3.
7. Stott SL, Hsu CH, Tsukrov DI, Yu M, Miyamoto DT, Waltman BA, et al. Isolation of circulating tumor cells using a microvortex-generating herringbone-chip. Proc Natl Acad Sci U S A 2010;107:18392–7.
8. Evans MJ, Smith-Jones PM, Wongvipat J, Navarro V, Kim S, Bander NH, et al. Noninvasive measurement of androgen receptor signaling with a positron-emitting radiopharmaceutical that targets prostate-specific membrane antigen. Proc Natl Acad Sci U S A 2011;108:9578–82.
9. Danila DC, Heller G, Gignac GA, Gonzalez-Espinoza R, Anand A, Tanaka E, et al. Circulating tumor cell number and prognosis in progressive castration-resistant prostate cancer. Clin Cancer Res 2007;13:7053–8.
10. Helo P, Cronin AM, Danila DC, Wenske S, Gonzalez-Espinoza R, Anand A, et al. Circulating prostate tumor cells detected by reverse transcription-PCR in men with localized or castration-refractory prostate cancer: concordance with CellSearch assay and association with bone metastases and with survival. Clin Chem 2009;55:765–73.

11. Kirby BJ, Jodari M, Loftus MS, Gakhar G, Pratt ED, Chanel-Vos C, et al. Functional characterization of circulating tumor cells with a prostate-cancer-specific microfluidic device. PLoS ONE 2012;7:e35976.
12. Stanbrough M, Bubley GJ, Ross K, Golub TR, Rubin MA, Penning TM, et al. Increased expression of genes converting adrenal androgens to testosterone in androgen-independent prostate cancer. Cancer Res 2006;66:2815–25.
13. Efstathiou E, Titus M, Tsavachidou D, Tzelepi V, Wen S, Hoang A, et al. Effects of abiraterone acetate on androgen signaling in castrate-resistant prostate cancer in bone. J Clin Oncol 2012;30:637–43.
14. Darshan MS, Loftus MS, Thadani-Mulero M, Levy BP, Escuin D, Zhou XK, et al. Taxane-induced blockade to nuclear accumulation of the androgen receptor predicts clinical responses in metastatic prostate cancer. Cancer Res 2011;71:6019–29.
15. Mendiratta P, Mostaghel E, Guinney J, Tewari AK, Porrello A, Barry WT, et al. Genomic strategy for targeting therapy in castration-resistant prostate cancer. J Clin Oncol 2009;27:2022–9.
16. Visakorpi T, Hyytinen E, Koivisto P, Tanner M, Keinanen R, Palmberg C, et al. *In vivo* amplification of the androgen receptor gene and progression of human prostate cancer. Nat Genet 1995;9:401–6.
17. Brown RS, Edwards J, Dogan A, Payne H, Harland SJ, Bartlett JM, et al. Amplification of the androgen receptor gene in bone metastases from hormone-refractory prostate cancer. J Pathol 2002; 198:237–44.
18. Wang Q, Li W, Zhang Y, Yuan X, Xu K, Yu J, et al. Androgen receptor regulates a distinct transcription program in androgen-independent prostate cancer. Cell 2009;138:245–56.
19. Cai C, He HH, Chen S, Coleman I, Wang H, Fang Z, et al. Androgen receptor gene expression in prostate cancer is directly suppressed by the androgen receptor through recruitment of lysine-specific demethylase 1. Cancer Cell 2011;20:457–71.
20. Carver BS, Chapinski C, Wongvipat J, Hieronymus H, Chen Y, Chandarlapaty S, et al. Reciprocal feedback regulation of PI3K and androgen receptor signaling in PTEN-deficient prostate cancer. Cancer Cell 2011;19:575–86.
21. Cai C, Chen S, Ng P, Bubley GJ, Nelson PS, Mostaghel EA, et al. Intratumoral *de novo* steroid synthesis activates androgen receptor in castration-resistant prostate cancer and is upregulated by treatment with CYP17A1 inhibitors. Cancer Res 2011;71:6503–13.
22. Ulmert D, Evans MJ, Holland JP, Rice SL, Wongvipat J, Pettersson K, et al. Imaging androgen receptor signaling with a radiotracer targeting free prostate-specific antigen. Cancer Discov 2012;2: 320–7.
23. Scher HI, Halabi S, Tannock I, Morris M, Sternberg CN, Carducci MA, et al. Design and end points of clinical trials for patients with progressive prostate cancer and castrate levels of testosterone: recommendations of the Prostate Cancer Clinical Trials Working Group. J Clin Oncol 2008;26:1148–59.
24. Text-ToFCS version 1.2.1. Available from: http://offsite.treestar.com/downloads/utilities/TextToFCS_documentation.

Science Translational Medicine AAAS

Inertial Focusing for Tumor Antigen–Dependent and –Independent Sorting of Rare Circulating Tumor Cells
Emre Ozkumur *et al.*
Sci Transl Med **5**, 179ra47 (2013);
DOI: 10.1126/scitranslmed.3005616

Editor's Summary

Positive and Negative Outcomes

Usually people want the good news first, to help cope with the bad news that inevitably follows. However, patients will soon desire both the positive and the negative outcomes together, according to the latest study by Ozkumur and colleagues. These authors have developed a multistage microfluidic device that is capable of sorting rare circulating tumor cells (CTCs) that are either positive or negative for the surface antigen epithelial cell adhesion molecule (EpCAM).

$EpCAM^+$ cells found in the bloodstream have long defined the typical CTC. Many sorting technologies have been developed to enumerate $EpCAM^+$ CTCs in cancer patient's blood; however, these cells are not always detectable in cancers with low EpCAM expression, like triple-negative breast cancer or melanoma. Ozkumur *et al.* engineered an automated platform, called the "CTC-iChip," that captured both $EpCAM^+$ and $EpCAM^-$ cancer cells in clinical samples using a series of debulking, inertial focusing, and magnetic separation steps. The sorted CTCs could then be interrogated using standard clinical protocols, such as immunocytochemistry. The authors tested the "positive mode" of their device using whole blood from patients with prostate, lung, breast, pancreatic, and colorectal cancers. After successfully separating out the $EpCAM^+$ CTCs, they confirmed that the cells were viable and had high-quality RNA for molecular analysis, in one example, detecting the *EML4-ALK* gene fusion in lung cancer. Using the "negative mode" of their device, the authors were able to capture $EpCAM^-$ CTCs from patients with metastatic breast cancer, pancreatic cancer, and melanoma. The isolated CTCs showed similar morphology when compared with primary tumor tissue from these patients, suggesting that the microfluidic device can be used for clinical diagnoses—delivering both positive and negative news at once.

Ozkumur *et al.* also demonstrated that CTCs isolated using the iChip could be analyzed on the single-cell level. One such demonstration with 15 CTCs from a prostate cancer patient reveals marked heterogeneity in the expression of mesenchymal and stem cell markers as well as typical prostate cancer –related antigens. The CTC-iChip can therefore process large volumes of patient blood to obtain not just $EpCAM^+$ CTCs but also the $EpCAM^-$ ones, thus giving a broader picture of an individual's cancer status and also allowing the device to be used for more cancer types. With the ability to further analyze the molecular characteristics of CTCs, this CTC-iChip could be a promising addition to current diagnostic tools used in the clinic.

Science Translational Medicine (print ISSN 1946-6234; online ISSN 1946-6242) is published weekly, except the last week in December, by the American Association for the Advancement of Science, 1200 New York Avenue NW, Washington, DC 20005.

CANCER DIAGNOSTICS

Inertial Focusing for Tumor Antigen–Dependent and –Independent Sorting of Rare Circulating Tumor Cells

Emre Ozkumur,[1]* Ajay M. Shah,[1]* Jordan C. Ciciliano,[2] Benjamin L. Emmink,[1] David T. Miyamoto,[2,3] Elena Brachtel,[4] Min Yu,[2,5] Pin-i Chen,[1] Bailey Morgan,[1] Julie Trautwein,[2] Anya Kimura,[2] Sudarshana Sengupta,[2] Shannon L. Stott,[1,2] Nezihi Murat Karabacak,[1] Thomas A. Barber,[1] John R. Walsh,[1] Kyle Smith,[1] Philipp S. Spuhler,[1] James P. Sullivan,[2,6] Richard J. Lee,[2,6] David T. Ting,[2,6] Xi Luo,[2,5] Alice T. Shaw,[2,6] Aditya Bardia,[2,6] Lecia V. Sequist,[2,6] David N. Louis,[4] Shyamala Maheswaran,[2,7] Ravi Kapur,[1] Daniel A. Haber,[2,5,6] Mehmet Toner[1,7†]

Circulating tumor cells (CTCs) are shed into the bloodstream from primary and metastatic tumor deposits. Their isolation and analysis hold great promise for the early detection of invasive cancer and the management of advanced disease, but technological hurdles have limited their broad clinical utility. We describe an inertial focusing–enhanced microfluidic CTC capture platform, termed "CTC-iChip," that is capable of sorting rare CTCs from whole blood at 10^7 cells/s. Most importantly, the iChip is capable of isolating CTCs using strategies that are either dependent or independent of tumor membrane epitopes, and thus applicable to virtually all cancers. We specifically demonstrate the use of the iChip in an expanded set of both epithelial and nonepithelial cancers including lung, prostate, pancreas, breast, and melanoma. The sorting of CTCs as unfixed cells in solution allows for the application of high-quality clinically standardized morphological and immunohistochemical analyses, as well as RNA-based single-cell molecular characterization. The combination of an unbiased, broadly applicable, high-throughput, and automatable rare cell sorting technology with generally accepted molecular assays and cytology standards will enable the integration of CTC-based diagnostics into the clinical management of cancer.

INTRODUCTION

The rarity of circulating tumor cells (CTCs) in the blood of cancer patients has required development of highly specialized technologies for their isolation (*1, 2*). Once detected, enumeration and molecular characterization of CTCs have been applied to prognostic classifications of breast, prostate, and colon cancers (*3*), and to predictive markers of targeted drug therapy in lung cancer (*4*). However, the limited sensitivity of commercially available approaches combined with the complexity and heterogeneity of the disease has restricted the broad acceptance and dissemination of CTC-based diagnostics (*5*).

Several strategies have been used to process blood for analysis of CTCs, including platforms for rapid scanning of unpurified cell populations (*6–8*). The most common enrichment approaches have used antibodies against the cell surface protein epithelial cell adhesion molecule (EpCAM). Labeling CTCs with anti-EpCAM–coated beads, followed by bulk magnetic enrichment methods (*9–11*), has been tested. The U.S. Food and Drug Administration (FDA)–approved Veridex system, CellSearch, immunomagnetically labels CTCs and then enriches the cells by bulk purification across a magnetic field. Conceptually, EpCAM-based CTC capture may have limited ability to identify tumor cells with reduced expression of this epithelial marker as a result of the epithelial-mesenchymal transition (EMT) (*12*). However, tumor antigen–independent CTC enrichment, such as bulk depletion of hematopoietic cells, suffers from poor yields and low purity (*13, 14*). Together, CTC isolation approaches have traditionally involved multiple batch processing steps, resulting in substantial loss of CTCs (*14*).

Recently, we introduced microfluidic methods to improve the sensitivity of CTC isolation (*15*), a strategy that is particularly attractive because it can lead to efficient purification of viable CTCs from unprocessed whole blood (*16–21*). The micropost CTC-Chip ($^{\mu P}$CTC-Chip) relies on laminar flow of blood cells through anti-EpCAM antibody-coated microposts (*15*), whereas the herringbone CTC-Chip (^{Hb}CTC-Chip) uses microvortices generated by herringbone-shaped grooves to direct cells toward antibody-coated surfaces (*16*). Although promising, these methods require surface functionalization to bind to tumor antigens on CTCs and thus yield CTCs that are immobilized within a microfluidic chamber and are not readily subjected to either standard clinical cytopathological imaging or single-cell molecular characterization.

To address the shortcomings of the current approaches, we developed a strategy that combines the strengths of microfluidics for rare cell handling while incorporating the benefits of magnetic-based cell sorting. After the magnetic labeling of cells in whole blood, this capture platform integrates three sequential microfluidic technologies within a single automated system: (i) debulking by separation of nucleated cells, including CTCs and white blood cells (WBCs), from red blood cells (RBCs) and platelets using deterministic lateral displacement (*22*); (ii) alignment of nucleated cells within a microfluidic channel using inertial focusing (*23*); and (iii) deflection of magnetically tagged cells into a collection

[1]Massachusetts General Hospital Center for Engineering in Medicine, Harvard Medical School, Boston, MA 02114, USA. [2]Massachusetts General Hospital Cancer Center, Harvard Medical School, Boston, MA 02114, USA. [3]Department of Radiation Oncology, Massachusetts General Hospital, Harvard Medical School, Boston, MA 02114, USA. [4]Department of Pathology, Massachusetts General Hospital, Harvard Medical School, Boston, MA 02114, USA. [5]Howard Hughes Medical Institute, Chevy Chase, MD 20815, USA. [6]Department of Medicine, Massachusetts General Hospital, Harvard Medical School, Boston, MA 02114, USA. [7]Department of Surgery, Massachusetts General Hospital, Harvard Medical School, Boston, MA 02114, USA.
*These authors contributed equally to this work.
†Corresponding author. E-mail: mtoner@hms.harvard.edu

channel. In essence, these three integrated microfluidic functions replace bulk RBC lysis and/or centrifugation, hydrodynamic sheath flow in flow cytometry, and magnetic-activated cell sorting (MACS). We call this integrated microfluidic system the CTC-iChip, based on the inertial focusing strategy, which allows positioning of cells in a near-single file line, such that they can be precisely deflected using minimal magnetic force. This integrated microfluidic platform, with its ability to isolate CTCs in suspension using both tumor antigen–dependent and tumor antigen–independent modes, is compatible with high-definition imaging and single-cell molecular analyses, as well as standard clinical cytopathology. We demonstrate its capabilities for diverse cancer diagnostic applications in both epithelial and nonepithelial cancers.

RESULTS

CTC-iChip design and function

The overall CTC-iChip isolation strategy is depicted in Fig. 1 and fig. S1. We explored two modes of immunomagnetic sorting to isolate CTCs: a positive selection mode (^{pos}CTC-iChip), whereby CTCs are identified and sorted on the basis of their expression of EpCAM, and a negative selection mode (^{neg}CTC-iChip), in which the blood sample is depleted of leukocytes by immunomagnetically targeting both the common leukocyte antigen CD45 and the granulocyte marker CD15.

Target cell labeling was developed and characterized for both operational modes (fig. S2). After labeling, the first stage within the CTC-iChip used hydrodynamic size–based sorting to achieve low shear microfluidic debulking of whole blood (*22*, *24*). RBCs, platelets, plasma proteins, and free magnetic beads were discarded, whereas nucleated cells (WBCs and CTCs) were retained and presented to the second stage for inertial focusing. The efficient removal of free beads is critical because these may accumulate in the magnetophoresis channel and significantly reduce the sensitivity and specificity of the approach. The operational principle of microfluidic debulking is based on hydrodynamic size–dependent deterministic lateral displacement (*22*, *24*), in which coincident flow of cell-containing and cell-free solutions through an array of microposts leads to rapid size-based separation (Fig. 1C and fig. S3). We tested two different array configurations with gaps between

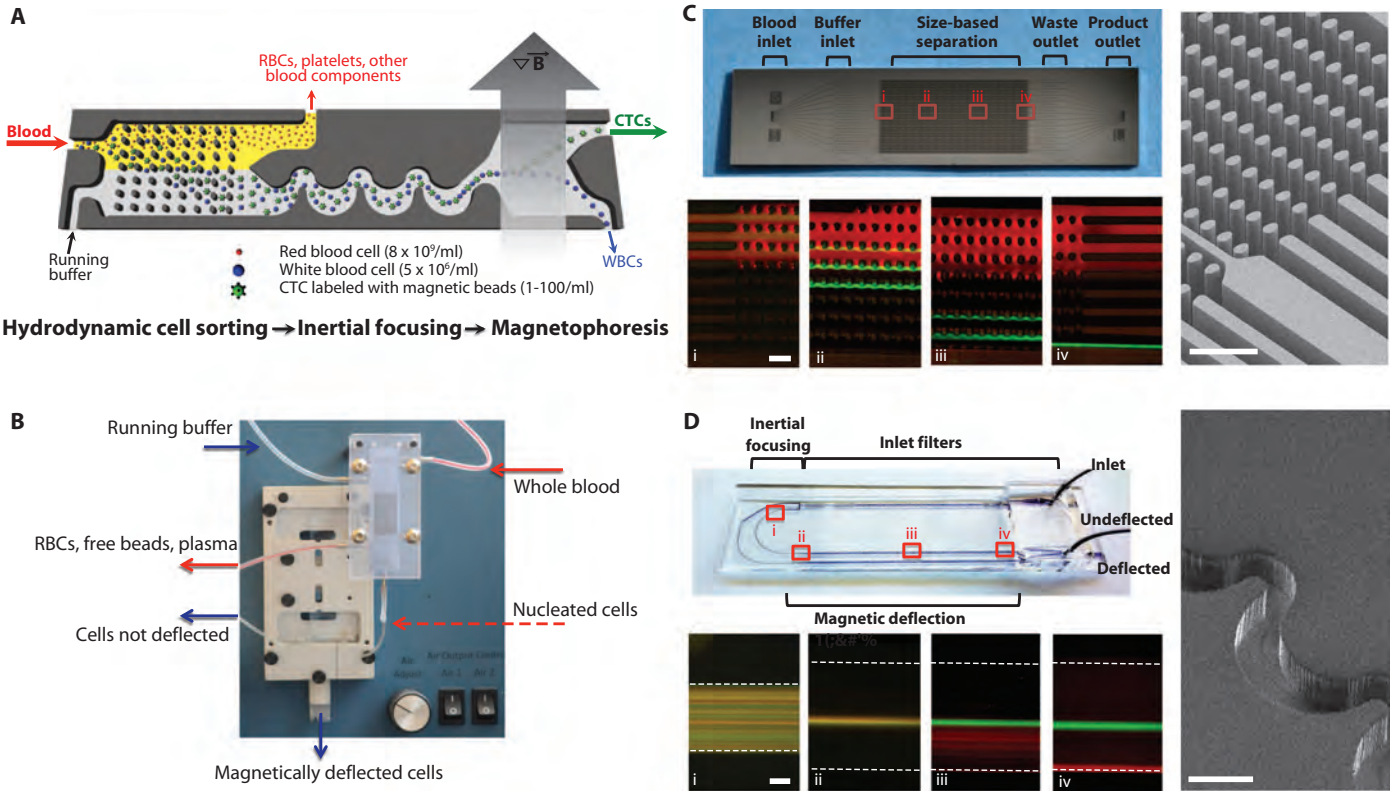

Fig. 1. The CTC-iChip system. (**A**) Three microfluidic components of the CTC-iChip are shown schematically. Whole blood premixed with immunomagnetic beads and buffer comprises the inputs. The figure demonstrates the positive isolation method; however, the system can be operated in negative depletion mode. (**B**) Integrated microfluidic system. The debulking array sits in a custom polycarbonate manifold that enables fluidic connections to the inputs, waste line, and second-stage microfluidic channels. The inertial focusing and magnetophoresis chip is placed in an aluminum manifold that houses the quadrupole magnetic circuit. Magnetically deflected cells are collected in a vial. (**C**) Hydrodynamic size–based sorting. A mixture of 2-μm (red) and 10-μm (green) beads enters the channel (i). Whereas the 2-μm beads remain in laminar flow and follow the fluid streamlines, the 10-μm spheres interact with the post-array (ii and iii) as shown in the scanning electron microscope (SEM) image (right panel). Larger beads are fully deflected into the coincident running buffer stream by the end of the array (iv). Scale bars, 100 μm. (**D**) Cell focusing and magnetophoretic sorting. Magnetically labeled SKBR3 (red) and unlabeled PC3-9 (green) cell populations are mixed and enter the channel in random distribution (i). After passing through 60 asymmetric focusing units (pictured in the SEM, right panel), the cells align in a single central stream (ii). Magnetically tagged cells are then deflected (iii) using an external magnetic field, and separation is achieved by the end of the channel (iv). Scale bars, 100 μm.

microposts of 20 or 32 μm. An array with 20-μm gaps retains virtually all nucleated cells with minimal contaminating RBCs but has a cutoff for cells larger than 21 μm and may therefore lose large CTCs or CTC clusters. In contrast, an array with 32-μm gaps has an extended operating range for cells between 8 and 30 μm but retains only 60% of WBCs. Because the cells lost in the 32-μm gap array are granulocytes and lymphocytes that are smaller than the reported CTC sizes (*16*), we selected this array for the CTC-iChip.

The second CTC-iChip component orders nucleated cells within the microfluidic channel, both laterally and longitudinally, so they can be precisely deflected into a collection channel with minimal magnetic moment. The rationale underlying the inertial focusing of cells in microchannels is based on the principles of pipe flow (*23*, *25*); essentially, a cellular fluid entering asymmetric, curved channels emerges as a tight row of individual cells traveling within a defined streamline position (Fig. 1D). We tested variable cell suspensions for focusing performance; WBCs as well as cancer cell lines were well focused within the operational parameters (hematocrit less than 0.4%; flow rate between 50 and 150 μl/min; nucleated cell concentration less than 3×10^6/ml) (fig. S4). Inertial focusing operational parameters were matched to output of the preceding debulking array, and the in-line integration of these complex microfluidic structures within the CTC-iChip thus avoided cell losses associated with commonly used batch processing strategies.

In the final CTC-iChip component, magnetically labeled cells are separated from unlabeled cells within a deflection channel. The precise control over cell position provided by inertial focusing prevents cellular collisions during magnetophoresis; therefore, cell displacement occurs as a predictable function of magnetic load. We modeled the forces exerted on cells labeled with 1-μm beads using a quadrupole magnetic circuit (fig. S5) and predicted deflection patterns under different flow and magnetic load conditions (Fig. 2A). This model was tested using magnetically labeled PC3-9 human prostate cancer cells. The measured deflection distance, plotted as a function of magnetic load, matched the prediction (Fig. 2B).

To demonstrate the dependence of sensitivity on flow speed, we processed labeled cells at various flow rates and quantified the number of beads per cell for deflected and nondeflected outputs (Fig. 2C and fig. S6). The improvement in sensitivity with increasing magnetic residence time (by reducing flow speed) correlated with the predictive model (Fig. 2D), indicating high magnetic sensitivity for the overall system (5 to 20 beads per cell, depending on cell size). The process parameters characterized for the ^{pos}CTC-iChip applied similarly to the ^{neg}CTC-iChip.

Evaluating the CTC-iChip using cells spiked into whole blood

To evaluate the efficiency of the CTC-iChip, we spiked five cell lines spanning a broad range of EpCAM expression into healthy whole blood and isolated using ^{pos}CTC-iChip or ^{neg}CTC-iChip modes. The EpCAM expression of each cell line was quantified by comparing the anti-EpCAM signal to that of a matched irrelevant antibody (Fig. 3A). Recovery of SKBR3 human breast cancer cells [24-fold EpCAM signal over control immunoglobulin G (IgG)] was 98.6 ± 4.3% (mean ± SD), and capture of human prostate PC3-9 cancer cells (3.7-fold EpCAM signal) was 89.7 ± 4.5% (Fig. 3B). Even cells with minimal EpCAM expression, such as MDA-MB-231 (*26*), a "triple-negative" mesenchymal breast

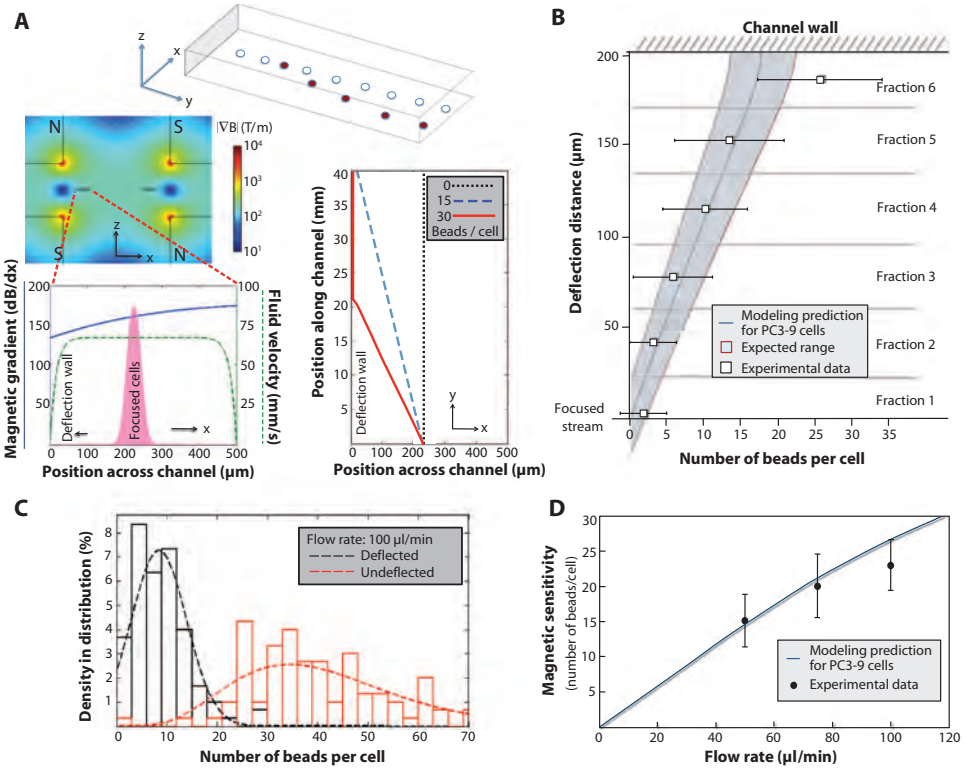

Fig. 2. Modeling and magnetic sensitivity of the system. (**A**) A mathematical model describes the deflection of labeled cells (red) from a focused stream (white). Finite element method analysis of the quadrupole magnetic circuit and fluid flow in the channel provided estimates of the magnetic gradient (blue) and flow rate (green) across the deflection channel (left panel). This information, in conjunction with our experimental understanding of cell position in the focused stream (pink), was used to construct an overall model to predict the trajectories of focused cells with varying magnetic loads (right panel). (**B**) High sensitivity of inertial focusing enhanced magnetophoresis. Human PC3-9 cells were labeled with varying numbers of magnetic beads and collected in separate exit streams after traveling in the 4-cm-long magnetic deflection channel, fractionating the cells based on magnetic deflection distance. The beads on a representative population of cells were counted in each fraction. The deflection distance was measured from focused stream position to the channel wall. Fraction 6 included cells that deflected all the way and traveled at the wall; therefore, this data point did not match the simulation. The expected variations in cell sizes and the initial distribution of cells in the focused stream contribute to a variation in the deflection pattern that is reflected by shading the expected range around the model prediction. (**C**) The experimental "magnetic sensitivity" was determined by plotting histograms of bead loading density for deflected and undeflected cells for a given flow rate. The intersection of curve fits of these data represents the minimum number of beads required to deflect a cell. (**D**) The minimum required magnetic load increases with higher flow rates, as expected, and is accurately predicted by the model.

cancer cell line (only 2.5-fold EpCAM signal over control), were recovered with 77.8 ± 7.8% capture efficiency by ^{pos}CTC-iChip. Virtually complete abrogation of EpCAM expression, achieved by ectopic expression of the EMT master regulator LBX1 in MCF10A human breast cancer cells (MCF10A-LBX1) (*27*), resulted in 10.9 ± 3.0% capture efficiency.

Switching to the ^{neg}CTC-iChip, both the epithelial parental MCF10A cells and their highly mesenchymal MCF10A-LBX1 derivatives were captured at equal efficiency (96.7 ± 1.9% for MCF10As and 97.0 ± 1.7% for the MCF10A-LBX1 derivatives) (Fig. 3B). Together, these two modes demonstrate the flexibility of the CTC-iChip to isolate a broad spectrum of rare cells with high efficiency in both tumor antigen–dependent and tumor antigen–independent modes.

Sample purity was analyzed for both operating modes. Using EpCAM-based positive selection, we achieved an average >3.5-log purification (mean, 1500 WBCs/ml of whole blood; range, 67 to 2537 WBCs/ml). In the leukocyte depletion mode, purification was 2.5 log (mean, 32,000 WBCs/ml; range, 17,264 to 39,172 WBCs/ml) (Fig. 3C). In the ^{pos}CTC-iChip, the vast majority of contaminating WBCs carried magnetic beads, suggesting that nonspecific interactions between WBCs and either the anti-EpCAM antibody or the beads themselves caused the contamination. In the ^{neg}CTC-iChip, contaminating WBCs were free of beads, suggesting that they comprise a population of leukocytes with reduced CD45 or CD15 expression, as confirmed by flow cytometry (table S1).

^{pos}CTC-iChip isolation of CTCs

We tested the ^{pos}CTC-iChip in patients with prostate cancer, a disease in which metastatic lesions primarily affect bone, and hence, CTC analysis is key to analyzing recurrences after resection of the primary tumor. On average, 10 ml (range, 6 to 12 ml) of whole blood was analyzed from these patients. Using triple staining for cytokeratins (CKs) (epithelial marker), CD45 (leukocytes), and 4′,6-diamidino-2-phenylindole (DAPI) (nuclear marker), we identified ≥0.5 CTC/ml in 37 of 41 (90%) prostate patients with recurrent (castration-resistant) disease (mean, 50.3/ml; range, 0.5 to 610/ml; median, 3.2/ml) (Fig. 4A). The detection cutoff of 0.5 CTC/ml was more than 2 SDs above the mean number of CK$^+$ cells detected in 13 healthy donors (excluding an outlier with 0.7/ml; mean ± SD, 0.17 ± 0.12/ml; median, 0.19/ml; range, 0 to 0.33/ml). WBC contamination in the ^{pos}CTC-iChip product was low (mean, 1188/ml; median, 352/ml; range, 58 to 9249/ml), resulting in high sample purities (mean, 7.8%; median, 0.8%; range for samples with ≥0.5 CTC/ml, 0.02 to 43%) (fig. S7).

We performed a detailed comparison of the ^{pos}CTC-iChip with the FDA-approved CellSearch system (Fig. 4B). To minimize reagent variability between platforms, we used anti-EpCAM capture as well as CK and CD45 staining antibodies from the same source, and consistent criteria were used to evaluate putative CTCs. CTCs were defined as DAPI$^+$/CD45$^-$/CK$^+$, and WBCs were defined as DAPI$^+$ or DAPI$^+$/CD45$^+$ events. Specimens from prostate (n = 19) and other cancers (breast, n = 12; pancreas, n = 6; colorectal, n = 2; lung, n = 2) were compared. Although both assays performed well with high CTC loads (>30 CTCs per 7.5 ml), at lower CTC numbers, there was a marked differential in capture efficiency. Among the 86% (36 of 42) of metastatic cancer patients with fewer than 30 CTCs/7.5 ml, the number of CK$^+$ CTCs isolated with the ^{pos}CTC-iChip was significantly higher in 22 cases (P < 0.001, paired t test analysis). The remaining 14 cases had CTCs below detection limits for both systems (Fig. 4B and table S2). Thus, the sensitivity of the CTC-iChip is particularly critical in patients with a lower CTC burden.

In addition to capturing more CTCs in patients with lower CTC burdens, the iChip isolates these cells in suspension, which in turn enables their immobilization on a standard glass slide for high-resolution imaging and standard clinical cytopathological examination (fig. S8), as well as simultaneous staining for multiple biomarkers (Fig. 4, C and D). Beyond imaging, molecular genetic tools are increasingly applied to the characterization of CTCs. Nowhere is this more evident than in non–small cell lung cancer (NSCLC), where targeted therapies can provide marked clinical benefit (*28*). Among the most challenging assays is detection of the *EML4-ALK* translocation in about 3% of cases, which marks those responsive to the selective

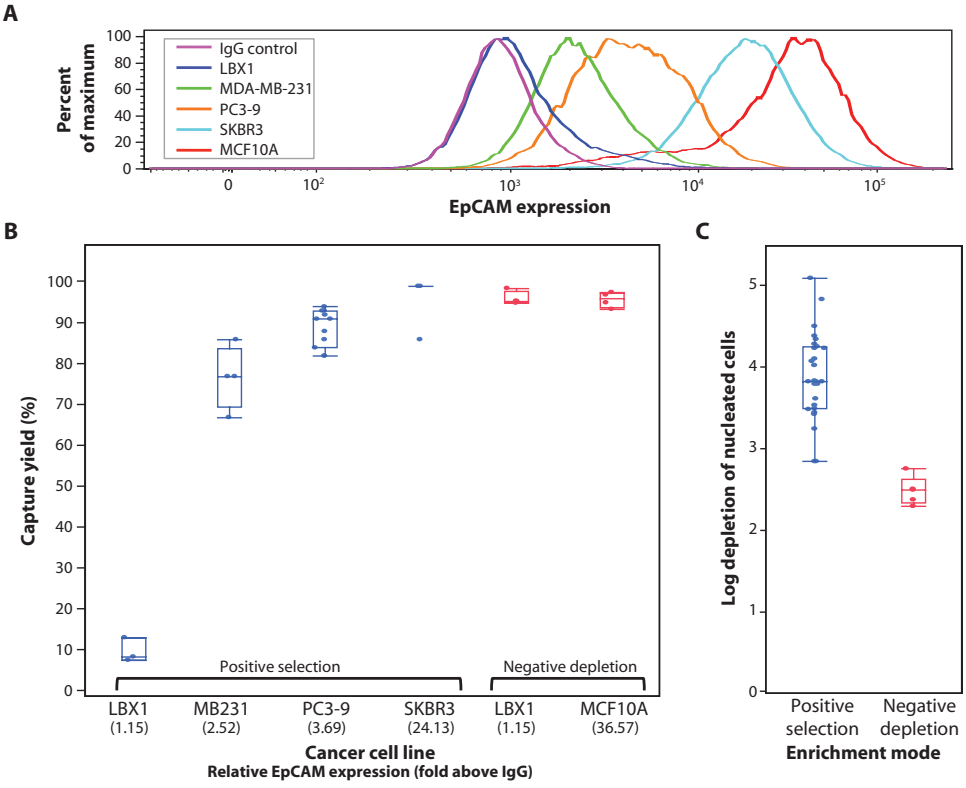

Fig. 3. Evaluation of overall system performance using cancer cell lines spiked into whole blood. (**A**) Quantitation of variable EpCAM expression in five cell lines using flow cytometry. (**B**) Capture yield of positive selection and negative depletion modes using various cell lines expressing different levels of EpCAM. (**C**) Background in ^{pos}CTC-iChip product is measured, achieving >3.5-log depletion of WBCs. In contrast, ^{neg}CTC-iChip has an order of magnitude lower purification. In both (B) and (C), each data point is an experimental result. Upper and lower bounds of the boxes signify the 75th and 25th quantiles, respectively. Perpendicular line in the box represents median value, and data points left above or below the error bars are outliers.

targeted inhibitor crizotinib. Detection of this intrachromosomal translocation by fluorescence in situ hybridization (FISH) is difficult, and, at the molecular level, the variability of chromosomal breakpoints necessitates RNA-based detection of the fusion transcript, which cannot be readily achieved using either fixed CTCs or free plasma nucleic acids.

We established a reverse transcription polymerase chain reaction (RT-PCR) assay capable of detecting the *EML4-ALK* translocation in H3122 lung cancer cells spiked into WBCs at a purity of 0.1% or introduced into whole blood (10 cells/10 ml) and processed through the ^{pos}CTC-iChip (Fig. 4E). In patient specimens, the *EML4-ALK* transcript was detected in CTCs from four cases known to have this chromosome rearrangement by FISH analysis of the primary tumor. It was absent in CTCs from two NSCLC patients and one patient with prostate cancer whose tumors were all known to lack this abnormality. In cases where CTC-based RNA analysis identified the expected product, nucleotide sequencing confirmed the breakpoint in the fusion transcript (Fig. 4F). Thus, the ^{pos}CTC-iChip allowed purification of CTCs for RNA-based molecular genotyping.

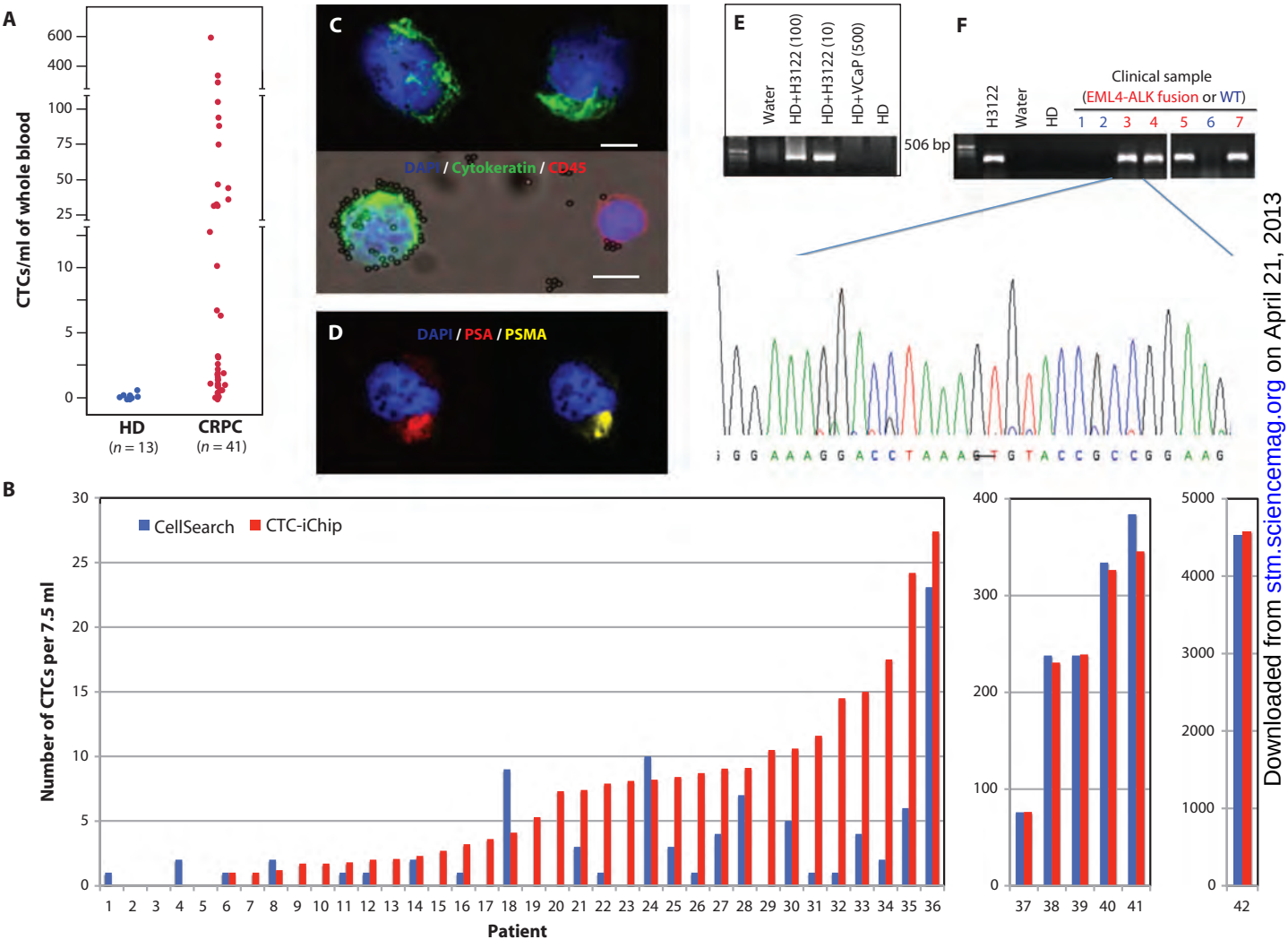

Fig. 4. CTC isolation by ^{pos}CTC-iChip in cancer patients. (**A**) CTCs isolated from castrate-resistant prostate cancer (CRPC) patients were enumerated and compared with blood specimens processed from healthy donors. (**B**) EpCAM-based isolation using ^{pos}CTC-iChip was compared with the CellSearch system. Clinical samples were metastatic cancer patients of prostate (n = 19), breast (n = 12), pancreas (n = 6), colorectal (n = 2), and lung (n = 2). All counts were normalized to 7.5 ml. (**C**) For enumeration of CTCs from CRPC patients, CK8/18/19 staining was used (green). CD45 antigen (red) was used to identify contaminating leukocytes. Scale bars, 10 μm. (**D**) A CTC from a CRPC patient was stained for prostate-specific antigen (PSA) (red), prostate-specific membrane antigen (PSMA) (yellow), and DAPI (blue) to demonstrate dual immunofluorescence staining for PSAs. (**E**) Validation of *EML4-ALK* RT-PCR assay was completed with cell lines. ^{pos}CTC-iChip products of whole blood from a healthy donor (HD) spiked with 0, 10, and 100 H3122 cells (expressing *EML4-ALK* variant 1) per 10 ml were subjected to RT-PCR for detection of the *EML4-ALK* fusion. Product isolated from healthy donor blood spiked with 500 VCaP cells/ml was processed as a negative control. (**F**) ^{pos}CTC-iChip products from patient samples known to harbor the *EML4-ALK* translocation by FISH were similarly processed as in (E), and the bands were sequenced to confirm the presence of the fusion transcript. A representative sequence trace from patient 3 shows the translocation breakpoint between exon 13 of *EML4* and exon 20 of *ALK*. CTC analysis of three patients whose cancer lacks the translocation was used to establish specificity: a prostate cancer patient (lane 1), an *EGFR* mutant lung cancer patient (lane 2), and a *HER2*-amplified lung cancer patient (lane 6).

^{neg}CTC-iChip to isolate CTCs

Given the heterogeneity of circulating cancer cells, including the subset thought to undergo EMT, depletion of normal blood cells from clinical specimens should allow characterization of unlabeled nonhematopoietic cells. We analyzed CTCs from 10 patients with metastatic breast cancer, including luminal (ER^+/PR^+, $n = 6$), triple-negative ($ER^-/PR^-/HER2^-$, $n = 2$), and $HER2^+$ ($n = 2$) subtypes. Triple-negative breast cancers are noteworthy in that they express primarily mesenchymal markers and are unlikely to be captured efficiently using positive selection for $EpCAM^+$ cells (*20*).

We stained the enriched CTC specimens using the Papanicolaou (Pap) stain, which is used for cytopathology analysis in clinical laboratories. In selected cases, the hematoxylin and eosin (H&E)–stained primary tumor tissue was compared with Pap-stained fine needle aspirates (FNAs) of the tumor or pleural effusions from the same patient. A remarkably similar morphological appearance was evident between cancer cells in the primary breast tumors and the isolated CTCs, as shown for three different patients in Fig. 5A. An ER^+ breast cancer patient revealed small and regularly shaped cells in H&E, cytology, and CTC samples. Similarly, larger and more irregular tumor cells were found in a $HER2^+$ primary breast cancer by H&E cytology and CTC analysis. In another example from a triple-negative high-grade breast cancer patient, pleomorphic CTCs similar to the patient's previously sampled cytology specimen were seen.

We extended these morphological analyses to pancreatic cancer and melanoma with similar findings (Fig. 5A). For these, pancreatic adenocarcinoma showed CTCs of comparable size to the primary tumor by both histology and Pap cytology. Conversely, melanoma consisted of dyshesive tumor cells. The spindled cytoplasm in melanoma was also

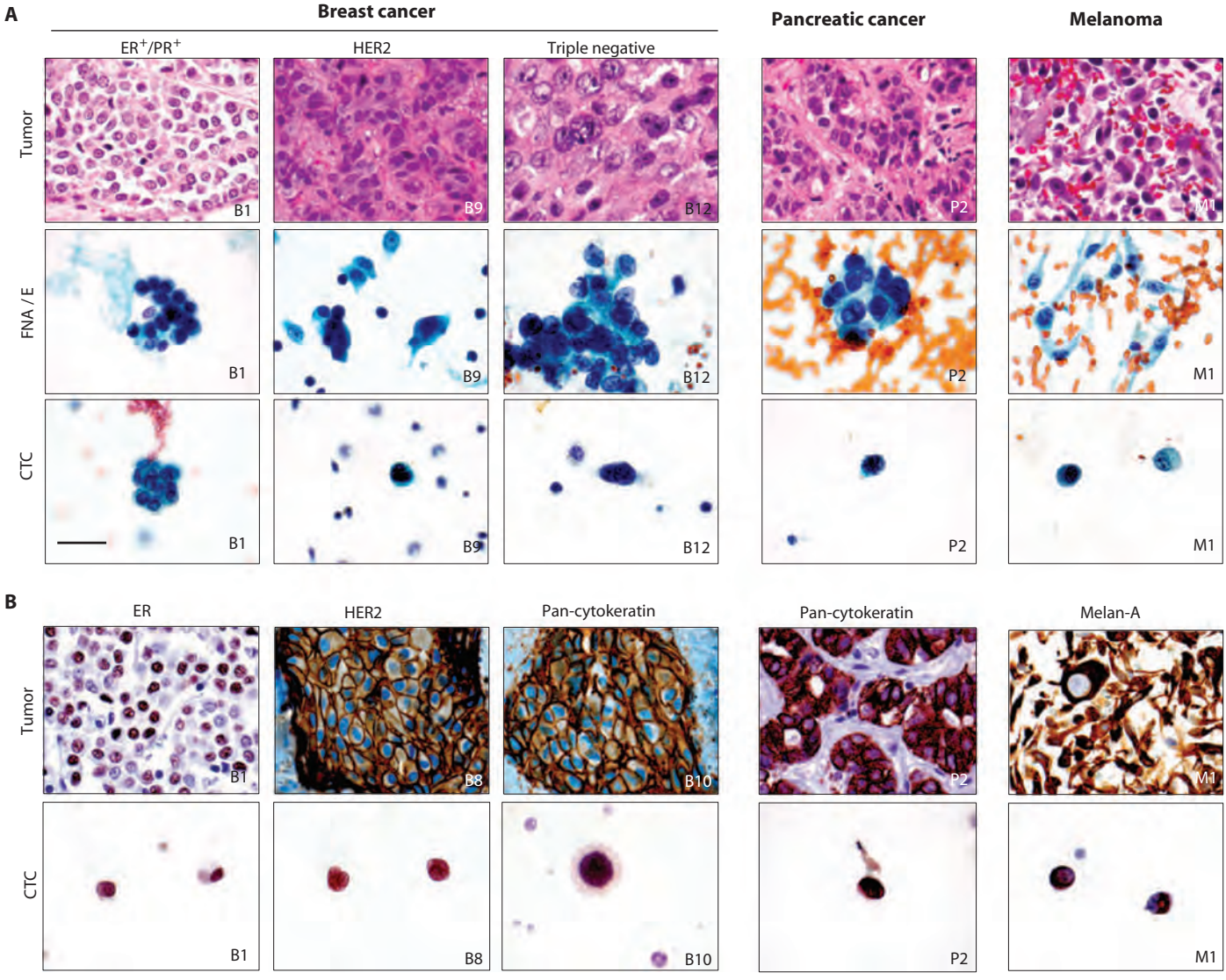

Fig. 5. Classification of CTCs with cytopathology and ICC. (**A**) Specimens from H&E-stained primary and metastatic tumors (upper row) are compared with matched Pap-stained cytology samples from FNAs or pleural effusions (FNA/E) (middle row) and Pap-stained CTCs enriched from blood samples of the same patient using ^{neg}CTC-iChip (lower row). Marked morphological similarity is seen between isolated CTCs and main tumors or cytology samples. (**B**) ICC profiles of primary and metastatic tumors (upper panel) matched to CTCs from the same patient (lower panel). All images: ×1000 original magnification. Scale bar is 30 μm and valid for all images.

seen on the cytology preparation, but the CTCs appeared round. As a neural crest–derived malignancy, melanoma cells do not express EpCAM, and hence, their detection requires the ^{neg}CTC-iChip isolation mode. Nevertheless, on the basis of established cellular and nuclear morphology criteria, our CTC analyses were considered to be of sufficient quality to enable a clinical diagnosis of suspicious for malignancy.

Pap-stained CTC slides were destained and then subjected to immunocytochemistry (ICC), which was first validated through cell lines (fig. S9). ICC of CTCs identified estrogen receptor (ER) protein in luminal breast cancer cells, keratin in triple-negative cells, and strong HER2 staining in cells from HER2$^+$ breast cancers (Fig. 5B and fig. S10). Similarly, CTCs from patients with pancreatic cancer stained positive by ICC for CK, and CTCs from melanoma patients stained positive for the melanocytic marker Melan-A (Fig. 5B and fig. S10). The combination of Pap staining followed by ICC enabled enumeration of CTCs isolated by ^{neg}CTC-iChip despite the presence of surrounding leukocytes.

Not all cytologically suspicious cells (for example, large cells with large, irregular nuclei as identified on the Pap-stained CTC slide) could be confirmed as tumor cells by ICC staining. Conversely, cells that were not scored as CTCs on initial cytological evaluation were subsequently identified as tumor cells by ICC, reflecting substantial heterogeneity in CTC size and morphology (fig. S11). Thus, by not relying exclusively on immunofluorescence-based scoring of CK$^+$ cells, we were able to apply to CTCs the same rigorous morphological and immunohistochemical criteria used by clinical cytopathologists in the diagnosis of malignancy.

We observed large variation in CTC size among different cancer types. Although some CTCs were larger than leukocytes, there was considerable overlap between the two cell populations (Fig. 6). The variation in CTC size was not restricted to different cancer histologies. In one patient with ER$^+$/PR$^+$ breast cancer whose CTCs were isolated using the ^{neg}CTC-iChip and analyzed using a combination of Pap stain and ICC, we identified CTCs ranging from 9 to 19 μm in diameter.

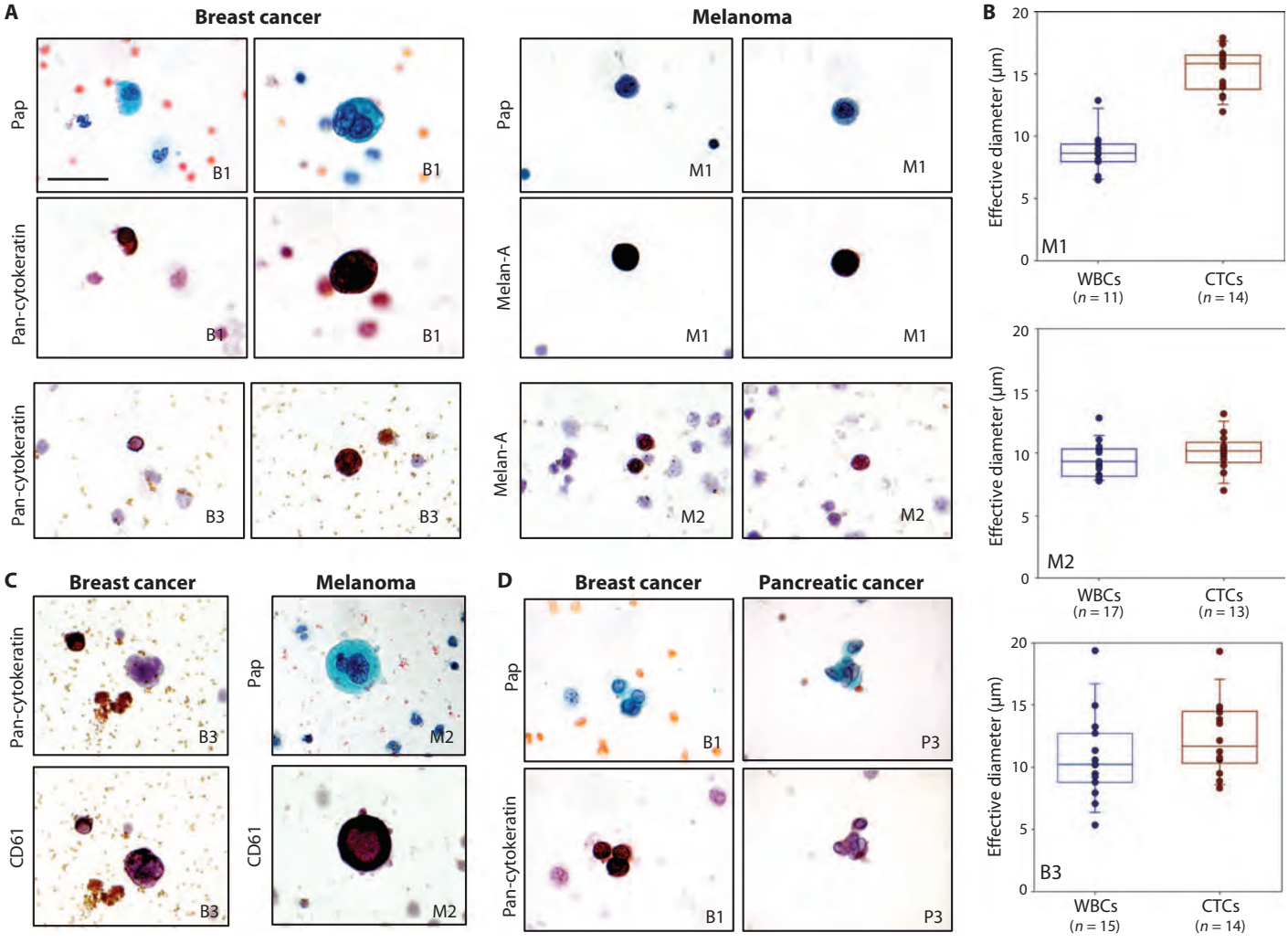

Fig. 6. Variation of CTC sizes and morphologies. (**A**) CTCs from breast cancer and melanoma patients consecutively stained with Pap and either anti-CK (breast) or anti–Melan-A (melanoma) antibodies. (**B**) Quantitative analysis of the effective diameter (maximum feret diameter) for individual cells isolated in three cases. The top two panels are from different melanoma patients (M1 and M2). The bottom panel is from a breast cancer patient (B3). (**C**) Occasional very large cells with ample cytoplasm and multilobed nuclei were initially considered suspicious but were CK$^-$. The same cells were subsequently restained for the platelet marker CD61, which supports their identification as circulating megakaryocytes. (**D**) CTCs were occasionally observed as clusters and confirmed by positive CK staining. All images: ×1000 original magnification. Scale bar, 30 μm.

Although most melanoma CTCs were large in size (>12 μm), one patient with metastatic melanoma had numerous CTCs less than 10 μm in diameter, detected using Pap and ICC for Melan-A (Fig. 6, A and B). In breast cancer and melanoma patients, some very large atypical cells (>30 μm) identified by Pap staining as having multilobed nuclei were at first assumed to be CTCs. However, ICC staining for the platelet marker CD61 confirmed their identity as megakaryocytes (Fig. 6C). Finally, application of the ^{neg}CTC-iChip platform identified clusters of two to six CK$^+$ CTCs in breast and pancreatic cancers, consistent with our previous detection of CTC clusters using the ^{Hb}CTC-Chip (*16*) (Fig. 6D). The negative selection mode of the CTC-iChip thus provided a comprehensive and unbiased view of nonhematological cells in the bloodstream of cancer patients.

Single-cell RNA expression in CTCs

Global CTC expression analyses may identify major pathways involved in metastasis (*20*), but the inherent heterogeneity of CTCs necessitates the identification of expression patterns and signaling pathways within individual cells. We therefore applied a series of single-cell micromanipulation approaches to interrogate individual CTCs isolated from a patient with prostate cancer using the ^{neg}CTC-iChip. Although micromanipulation approaches require expertise and can be time-consuming, the fact that the CTCs are unadulterated allows for more accurate RNA-based expression profiling than isolated fixed cells. EpCAM$^+$ CTCs were distinguished from contaminating CD45$^+$ leukocytes within the ^{neg}CTC-iChip product by immunostaining (Fig. 7, A and B). CTCs identified as EpCAM$^+$/CD45$^-$ were individually isolated and subjected to RNA analysis by multigene microfluidic quantitative RT-PCR (qRT-PCR), profiling for a panel of transcripts implicated in androgen receptor (AR) signaling, cellular proliferation, stem cell, epithelial and mesenchymal cell fates, and leukocyte-specific lineage (Fig. 7C). Single cells from the human prostate cancer cell line LNCaP were used to optimize assay conditions (fig. S12).

A marked heterogeneity was apparent among 15 CTCs isolated from a single patient with metastatic CRPC who had progressed through multiple lines of therapy, including androgen deprivation therapy with leuprolide, the chemotherapeutic drug docetaxel, and the second-line androgen biosynthesis inhibitor abiraterone acetate. Consistent with EpCAM$^+$ immunostaining, 13 of the 15 CTCs were positive for epithelial gene expression, of which 2 CTCs were dual positive for epithelial as well as mesenchymal markers vimentin and N-cadherin (Fig. 7D). Thus, a subset of CTCs appears to have undergone partial EMT. CTC heterogeneity was also evident with expression of stem cell markers [Nanog, Oct-4 (POU5F1), and c-Myc] in 10 of the 15 CTCs, which overlapped primarily with epithelial markers within individual CTCs (Fig. 7C). Proliferation markers cyclin B, cyclin D, Aurora A kinase, and MYBL2 were detected in another subset of seven CTCs.

AR activity, previously defined in CTCs as the ratio of androgen-driven PSA to androgen-repressed PSMA expression (*21*), was heterogeneous among CTCs. The "AR on" phenotype (PSA expression only) was only seen in 2 of the 15 CTCs, whereas the "AR-off" state (PSMA only) was evident in 2 CTCs, and the "mixed AR" state (PSA$^+$/PSMA$^+$) in 10 CTCs (Fig. 7D). This distribution is concordant with single-cell immunofluorescence analysis of AR signaling status in CTCs from patients with CRPC (*21*).

DISCUSSION

The CTC-iChip described here has the ability to process large volumes of whole blood (8 ml/hour), with high throughput (10^7 cells/s) and

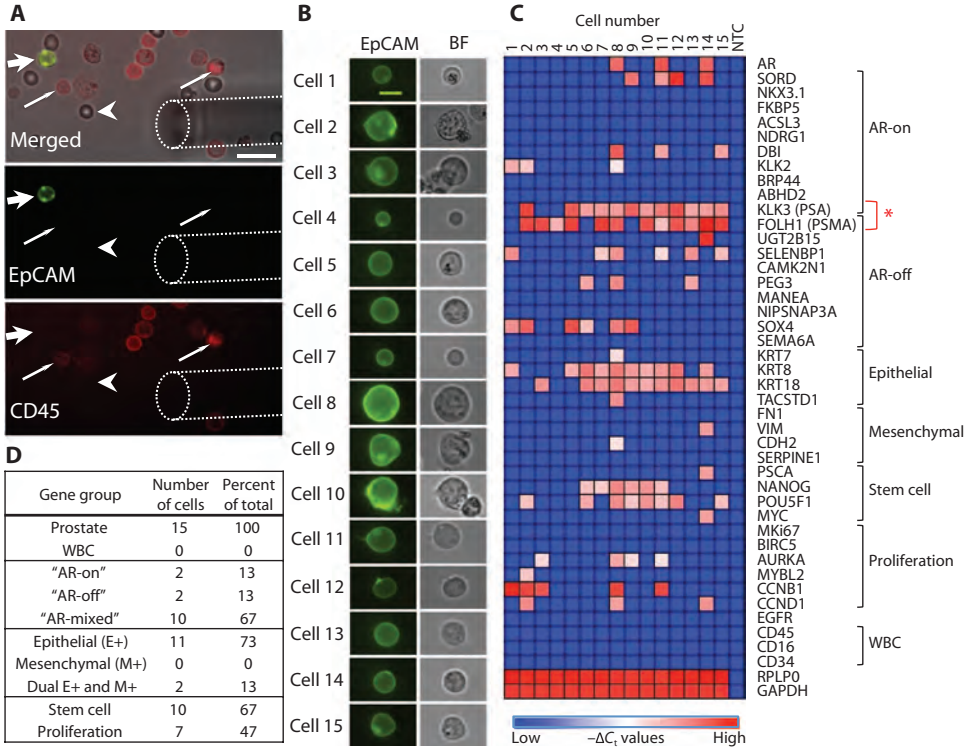

D

Gene group	Number of cells	Percent of total
Prostate	15	100
WBC	0	0
"AR-on"	2	13
"AR-off"	2	13
"AR-mixed"	10	67
Epithelial (E+)	11	73
Mesenchymal (M+)	0	0
Dual E+ and M+	2	13
Stem cell	10	67
Proliferation	7	47

Fig. 7. Heterogeneity of RNA expression between CTCs isolated from a prostate cancer patient. (**A**) Micromanipulation of single CTCs isolated from a blood specimen of a patient with prostate cancer using the ^{neg}CTC-iChip and stained in solution with anti-EpCAM (green) and anti-CD45 (red) antibodies. Top panel shows a bright-field image merged. Wide arrow points to an EpCAM$^+$/CD45$^-$ CTC. Thin arrow points to EpCAM$^-$/CD45$^+$ leukocytes. Arrowhead denotes an erythrocyte. Dashed line outlines the micromanipulator needle tip. Bottom two panels show distinct imaging channels. Scale bar, 20 μm. (**B**) EpCAM and bright-field images of 15 single prostate cancer CTCs from a single patient selected for transcriptional profiling. Scale bar, 10 μm. (**C**) Heat map of normalized gene expression ($-\Delta C_t$) of 43 genes in each of the single CTCs measured by microfluidic qRT-PCR. Columns list each individual prostate CTC, and rows show the panel of genes assayed, grouped thematically. The red asterisk highlights the gene expression patterns of PSA and PSMA, which provide a measure of AR signaling activity. NTC, no-template control. (**D**) Table listing the proportional distribution of various gene groups expressed in single CTCs isolated from the prostate cancer patient.

at high efficiency, in positive selection (tumor antigen–dependent) and negative depletion (tumor antigen–independent) modes, thus enabling cytopathological and molecular characterization of both epithelial and nonepithelial cancers. Traditional magnetophoresis requires the attachment of either hundreds of beads per cell or very large beads to provide sufficient magnetic moment for cell isolation (*11, 29*). In contrast, by virtue of its ability to precisely position cells within the channel using inertial focusing, the fluidic design of the CTC-iChip allows for efficient fractionation of cells with only a few 1-μm beads, resulting in high yields and purity of CTC isolation.

We have tested initial "proof-of-principle" clinical applications of both the positive and negative selection modes of the CTC-iChip. The ^{pos}CTC-iChip isolated CTCs at a purity of >0.1%, which is sufficient for molecular analyses, including detection of the *EML4-ALK* fusion transcript in NSCLC. Total CTC capture yield is critical to both genotyping and other applications, including enumeration for either prognostic or drug response measurements. The median number of CTCs detected by CK staining of ^{pos}CTC-iChip product was 3.2 CTCs/ml, with 90% of clinical samples having CK^+ cells above the threshold set using healthy donors. In a similar cohort using the CellSearch system, a median of 1.7 CTCs/ml was detected, with 57% of samples above the threshold (*30*). In our direct comparison between the ^{pos}CTC-iChip and the CellSearch system, the microfluidic device was significantly more sensitive at low CTC numbers (<30 CTC/7.5 ml). These results suggest that a subpopulation of $EpCAM^{low}$ cells was missed by the CellSearch bulk processing approach. Thus, whereas current commercially available approaches may be effective in patients with $EpCAM^{hi}$ CTCs, the CTC-iChip displayed increased sensitivity for patients with low numbers of circulating cancer cells, which may also have $EpCAM^{low}$ expression.

Previously, we demonstrated the efficacy of two microfluidic systems to isolate CTCs from whole blood. CK^+ CTCs were detected in 99% of patients with high purity (18 to 70%) in the first-generation micropost chip (*15*), and application of disease-specific markers for staining (PSA) and computer-assisted enumeration methods were later found to improve system reliability and specificity (*19*). Building on the improved heuristics and staining, CTCs were subsequently detected in 64% of prostate patients using the first-generation micropost chip (*19*), and in 93% of patients using the second-generation herringbone chip (*16*). Yet, these systems remain limited by low throughput (~1 to 2 ml of blood/hour), the inability to conduct single-cell or slide-based analyses, the requirement for three-dimensional image scanning platforms, and the availability of only a positive selection mode. The CTC-iChip system presented here thus encompasses major advances over our previous methods. Whole blood is now processed through a microscale system at speeds comparable to bulk systems (8 ml/hour) while preserving the high sensitivity afforded by microfluidic isolation techniques. Furthermore, rapid and gentle isolation of CTCs, as well as their collection in suspension, increases the integrity of these cells and their RNA quality, which are crucial for downstream analyses, such as cytopathology and single-cell expression profiling.

Moreover, the system can be run in either a positive selection or a negative depletion mode, thus broadening its potential application in the clinic and in basic research studies. The ^{neg}CTC-iChip allows for depletion of normal blood cells, uncovering an unselected population of nonhematopoietic cells for analysis. The robustness of this platform was demonstrated by staining CTCs per clinical pathology protocols, which yielded high-quality diagnostic images. The ^{neg}CTC-iChip allowed for isolation of CTCs from a nonepithelial cancer (melanoma) and from cancer that has undergone EMT and lost virtually all detectable EpCAM expression (triple-negative breast cancer). Hence, the ^{neg}CTC-iChip will be broadly applicable to all cancers that demonstrate vascular invasion, a major limitation of current technologies.

However, several additional optimizations should be considered before the CTC-iChip technology can be deployed for large-scale clinical applications. These include further improvements in CTC purity to facilitate routine molecular analyses of CTCs and in total blood volume processed to enable early cancer detection. From a manufacturing standpoint, we envision the CTC-iChip being integrated into a single monolithic device made of plastic and incorporating all three components of the CTC-iChip within a single footprint. Integration of such an economical chip into a fully automated device would potentially enable broad dissemination of this technology.

The emerging field of CTC biology brings with it unprecedented insight into the mechanisms underlying the blood-borne metastasis of cancer, as well as powerful new clinical applications to help diagnose and manage disease. As the technology matures, these are likely to include the initial genotyping and molecular characterization of cancer, as well as repeated noninvasive sampling of tumors during treatment. Because targeted therapies increasingly shape the clinical paradigm of cancer therapeutics, such serial "real-time" monitoring of cancer for indicators of drug response and emerging resistance is likely to become a mainstay of clinical oncology. The integrated microfluidic technology platform presented here provides a major step in this direction by enabling processing of large blood volumes with high throughput and efficiency, isolating CTCs regardless of tumor surface epitopes, and providing an end product that is compatible with both standardized clinical diagnostics and advanced molecular analyses. Because rare cell detection technologies continue to improve in sensitivity, they may ultimately provide novel approaches for early detection of invasive cancer before the establishment of metastatic disease.

MATERIALS AND METHODS

Samples

MDA-MB-231, SKBR3, and MCF10A cell lines were obtained from the American Type Culture Collection. PC3-9 cells were obtained from Veridex, LLC, and LBX1-expressing MCF10A cells were derived from a stable cell line previously published by our laboratory (*27*). Device performance was evaluated by prelabeling the cell lines with a fluorescent marker and spiking them into whole blood at ~200 to 1000/ml of whole blood (Supplementary Materials and Methods).

Fresh whole blood was collected from healthy volunteers under an Institutional Review Board (IRB)–approved protocol or commercially sourced from Research Blood Components. Samples from metastatic breast, colorectal, pancreas, lung, melanoma, and prostate cancer patients were collected under a separate IRB-approved protocol.

Chip design and fabrication

Hydrodynamic sorting chips were designed at Massachusetts General Hospital (MGH) and fabricated by Silex with deep reactive ion etching on silicon wafers. The chip was sealed with anodically bonded glass cover to form the microfluidic chamber. A custom polycarbonate manifold was used to form the fluidic connections to the microchip (fig. S3). The

inertial focusing and magnetophoresis chips were designed and fabricated at MGH with soft lithography and polydimethylsiloxane (fig. S4). The chip was placed within a custom stainless steel manifold that held four magnets in a quadrupole configuration to create a magnetic circuit enabling cell deflection (fig. S5) (Supplementary Materials and Methods).

Magnetic bead labeling of target cells in whole blood

Before processing the whole blood, samples were incubated with functionalized magnetic beads 1 μm in diameter (Dynal MyOne 656-01, Life Technologies) (fig. S2). For ^{pos}CTC-iChip, beads were functionalized with a biotinylated anti-EpCAM antibody, and active magnetic mixing was applied to achieve good labeling of EpCAM^{low} cell lines. For negative depletion, anti-CD45 and anti-CD15 functionalized beads were used (Supplementary Materials and Methods).

Immunofluorescence staining of CTCs

For enumeration analysis, isolated cells were incubated with saponin, DAPI, and anti-CK [phycoerythrin (PE)] and anti-CD45 [allophycocyanin (APC)] antibodies, acquired from Veridex, still in suspension. Cells were plated on a poly-L-lysine–functionalized glass slide with a closed chamber (fig. S8), and glass slide was scanned with the BioView imaging system while the chamber was still intact. Cells that were CK$^+$/DAPI$^+$/CD45$^-$ were scored as CTCs. Samples evaluated for PSA/PSMA expression were stained with a primary/secondary approach. All antibodies are catalogued in table S3.

Comparison to CellSearch

For the CellSearch and ^{pos}CTC-iChip comparison, two blood tubes were drawn: one CellSave tube for CellSearch run and one EDTA tube for ^{pos}CTC-iChip run. Samples in CellSave tubes were processed within 3 days after the draw as optimized and recommended for CellSearch approach, and EDTA samples were processed with the ^{pos}CTC-iChip within 4 hours of draw. CellSearch product was scanned in Magnest cartridges with CellTracks system. ^{pos}CTC-iChip product was plated and scanned with the BioView system.

RT-PCR analysis

RNA isolation was done with RNeasy Micro Kit (Qiagen). After RNA isolation, reverse transcription of RNA to complementary DNA (cDNA) using oligo(dT) was performed with SuperScript III First-Strand Synthesis System for RT-PCR (Invitrogen). For detection of *EML4-ALK* fusion cDNAs, partial nested PCR analysis was done with FideliTaq PCR Master Mix (Affymetrix). PCR amplification was performed in a thermocycler (Peltier Thermal Cycler, MJ Research). Gel electrophoresis was done with an aliquot of RT-PCR products. The amplified *EML4-ALK* products were sequenced, and results were analyzed with the ABI PRISM DNA sequence analysis software (Applied Biosystems) (Supplementary Materials and Methods).

Cytology and ICC

CTCs were enriched via ^{neg}CTC-iChip from the whole blood of cancer patients and plated on a poly-L-lysine surface (fig. S8). Plating chamber was removed after cell adhesion to facilitate standard cytopathology processing. Pap stain was done with hematoxylin, eosin-azure, and orange G and initially reviewed for suspicious cells by a certified cytotechnologist (N. Hartford, MGH) and then formally reviewed by a staff cytopathologist (E.B.). Slides were then destained and exposed to ICC process (Supplementary Materials and Methods).

Single-cell micromanipulation and qRT-PCR

Blood samples from a patient with metastatic prostate cancer were processed through the ^{neg}CTC-iChip, and unfixed CTCs and contaminating leukocytes were stained in solution with fluorophore-conjugated antibodies against EpCAM and CD45. Single CTCs were identified based on an EpCAM$^+$/CD45$^-$ phenotype and transferred under direct microscopic visualization to individual PCR tubes with a TransferMan NK2 micromanipulator (Eppendorf AG). Single-cell cDNA was prepared and amplified for single-cell transcriptome analysis, followed by specific target preamplification (Fluidigm Corp.). Microfluidic qRT-PCR was performed with the BioMark Real-Time PCR system (Fluidigm Corp.). The normalized gene expression in each cell ($-\Delta C_t$) was calculated as the negative of the difference between the C_t value for each gene and the *GAPDH* C_t value for the cell. Heat maps of normalized gene expression ($-\Delta C_t$) were generated with the Heat Map image module of GenePattern, with global color normalization.

SUPPLEMENTARY MATERIALS

www.sciencetranslationalmedicine.org/cgi/content/full/5/179/179ra47/DC1
Materials and Methods
Fig. S1. CTC-iChip system details.
Fig. S2. Optimization of labeling in whole blood.
Fig. S3. Hydrodynamic size–based separation.
Fig. S4. Inertial focusing and magnetophoresis channels.
Fig. S5. Magnetic configuration.
Fig. S6. Beads per cell distribution in deflected and undeflected outputs.
Fig. S7. WBC contamination in ^{pos}CTC-iChip.
Fig. S8. Cell plating chamber.
Fig. S9. ICC stain validation through cell lines.
Fig. S10. Additional images of ICC-stained cells.
Fig. S11. Comparison of cell identification through Pap and ICC.
Fig. S12. Single-cell qRT-PCR optimization using cell lines.
Table S1. Contaminating cells in the ^{neg}CTC-iChip product are leukocytes.
Table S2. CellSearch versus ^{pos}CTC-iChip comparison.
Table S3. Antibodies used throughout the study.

REFERENCES AND NOTES

1. K. Pantel, R. H. Brakenhoff, B. Brandt, Detection, clinical relevance and specific biological properties of disseminating tumour cells. *Nat. Rev. Cancer* **8**, 329–340 (2008).
2. M. Yu, S. Stott, M. Toner, S. Maheswaran, D. A. Haber, Circulating tumor cells: Approaches to isolation and characterization. *J. Cell Biol.* **192**, 373–382 (2011).
3. M. C. Miller, G. V. Doyle, L. W. Terstappen, Significance of circulating tumor cells detected by the cellsearch system in patients with metastatic breast colorectal and prostate cancer. *J. Oncol.* **2010**, 617421 (2010).
4. S. Maheswaran, L. V. Sequist, S. Nagrath, L. Ulkus, B. Brannigan, C. V. Collura, E. Inserra, S. Diederichs, A. J. Iafrate, D. W. Bell, S. Digumarthy, A. Muzikansky, D. Irimia, J. Settleman, R. G. Tompkins, T. J. Lynch, M. Toner, D. A. Haber, Detection of mutations in *EGFR* in circulating lung-cancer cells. *N. Engl. J. Med.* **359**, 366–377 (2008).
5. J. M. Lang, B. P. Casavant, D. J. Beebe, Circulating tumor cells: Getting more from less. *Sci. Transl. Med.* **4**, 141ps13 (2012).
6. R. T. Krivacic, A. Ladanyi, D. N. Curry, H. B. Hsieh, P. Kuhn, D. E. Bergsrud, J. F. Kepros, T. Barbera, M. Y. Ho, L. B. Chen, R. A. Lerner, R. H. Bruce, A rare-cell detector for cancer. *Proc. Natl. Acad. Sci. U.S.A.* **101**, 10501–10504 (2004).
7. D. Marrinucci, K. Bethel, A. Kolatkar, M. S. Luttgen, M. Malchiodi, F. Baehring, K. Voigt, D. Lazar, J. Nieva, L. Bazhenova, A. H. Ko, W. M. Korn, E. Schram, M. Coward, X. Yang, T. Metzner, R. Lamy, M. Honnatti, C. Yoshioka, J. Kunken, Y. Petrova, D. Sok, D. Nelson, P. Kuhn, Fluid biopsy in patients with metastatic prostate, pancreatic and breast cancers. *Phys. Biol.* **9**, 016003 (2012).
8. D. Issadore, J. Chung, H. Shao, M. Liong, A. A. Ghazani, C. M. Castro, R. Weissleder, H. Lee, Ultrasensitive clinical enumeration of rare cells ex vivo using a micro-Hall detector. *Sci. Transl. Med.* **4**, 141ra92 (2012).
9. S. Miltenyi, W. Müller, W. Weichel, A. Radbruch, High gradient magnetic cell separation with MACS. *Cytometry* **11**, 231–238 (1990).

10. G. Deng, M. Herrler, D. Burgess, E. Manna, D. Krag, J. F. Burke, Enrichment with anti-cytokeratin alone or combined with anti-EpCAM antibodies significantly increases the sensitivity for circulating tumor cell detection in metastatic breast cancer patients. *Breast Cancer Res.* **10**, R69 (2008).
11. A. H. Talasaz, A. A. Powell, D. E. Huber, J. G. Berbee, K. H. Roh, W. Yu, W. Xiao, M. M. Davis, R. F. Pease, M. N. Mindrinos, S. S. Jeffrey, R. W. Davis, Isolating highly enriched populations of circulating epithelial cells and other rare cells from blood using a magnetic sweeper device. *Proc. Natl. Acad. Sci. U.S.A.* **106**, 3970–3975 (2009).
12. R. Kalluri, R. A. Weinberg, The basics of epithelial-mesenchymal transition. *J. Clin. Invest.* **119**, 1420–1428 (2009).
13. O. Lara, X. Tong, M. Zborowski, J. J. Chalmers, Enrichment of rare cancer cells through depletion of normal cells using density and flow-through, immunomagnetic cell separation. *Exp. Hematol.* **32**, 891–904 (2004).
14. L. Yang, J. C. Lang, P. Balasubramanian, K. R. Jatana, D. Schuller, A. Agrawal, M. Zborowski, J. J. Chalmers, Optimization of an enrichment process for circulating tumor cells from the blood of head and neck cancer patients through depletion of normal cells. *Biotechnol. Bioeng.* **102**, 521–534 (2009).
15. S. Nagrath, L. V. Sequist, S. Maheswaran, D. W. Bell, D. Irimia, L. Ulkus, M. R. Smith, E. L. Kwak, S. Digumarthy, A. Muzikansky, P. Ryan, U. J. Balis, R. G. Tompkins, D. A. Haber, M. Toner, Isolation of rare circulating tumour cells in cancer patients by microchip technology. *Nature* **450**, 1235–1239 (2007).
16. S. L. Stott, C. H. Hsu, D. I. Tsukrov, M. Yu, D. T. Miyamoto, B. A. Waltman, S. M. Rothenberg, A. M. Shah, M. E. Smas, G. K. Korir, F. P. Floyd Jr., A. J. Gilman, J. B. Lord, D. Winokur, S. Springer, D. Irimia, S. Nagrath, L. V. Sequist, R. J. Lee, K. J. Isselbacher, S. Maheswaran, D. A. Haber, M. Toner, Isolation of circulating tumor cells using a microvortex-generating herringbone-chip. *Proc. Natl. Acad. Sci. U.S.A.* **107**, 18392–18397 (2010).
17. S. Wang, K. Liu, J. Liu, Z. T. F. Yu, X. Xu, L. Zhao, T. Lee, E. K. Lee, J. Reiss, Y.-K. Lee, L. W. K. Chung, J. Huang, M. Rettig, D. Seligson, K. N. Duraiswamy, C. K. Shen, H. R. Tseng, Highly efficient capture of circulating tumor cells by using nanostructured silicon substrates with integrated chaotic micromixers. *Angew. Chem. Int. Ed. Engl.* **50**, 3084–3088 (2011).
18. U. Dharmasiri, S. K. Njoroge, M. A. Witek, M. G. Adebiyi, J. W. Kamande, M. L. Hupert, F. Barany, S. A. Soper, High-throughput selection, enumeration, electrokinetic manipulation, and molecular profiling of low-abundance circulating tumor cells using a microfluidic system. *Anal. Chem.* **83**, 2301–2309 (2011).
19. S. L. Stott, R. J. Lee, S. Nagrath, M. Yu, D. T. Miyamoto, L. Ulkus, E. J. Inserra, M. Ulman, S. Springer, Z. Nakamura, A. L. Moore, D. I. Tsukrov, M. E. Kempner, D. M. Dahl, C. L. Wu, A. J. Iafrate, M. R. Smith, R. G. Tompkins, L. V. Sequist, M. Toner, D. A. Haber, S. Maheswaran, Isolation and characterization of circulating tumor cells from patients with localized and metastatic prostate cancer. *Sci. Transl. Med.* **2**, 25ra23 (2010).
20. M. Yu, A. Bardia, B. S. Wittner, S. L. Stott, M. E. Smas, D. T. Ting, S. J. Isakoff, J. C. Ciciliano, M. N. Wells, A. M. Shah, K. F. Concannon, M. C. Donaldson, L. V. Sequist, E. Brachtel, D. Sgroi, J. Baselga, S. Ramaswamy, M. Toner, D. A. Haber, S. Maheswaran, Circulating breast tumor cells exhibit dynamic changes in epithelial and mesenchymal composition. *Science* **339**, 580–584 (2013).
21. D. T. Miyamoto, R. J. Lee, S. L. Stott, D. T. Ting, B. S. Wittner, M. Ulman, M. E. Smas, J. B. Lord, B. W. Brannigan, J. Trautwein, N. H. Bander, C. L. Wu, L. V. Sequist, M. R. Smith, S. Ramaswamy, M. Toner, S. Maheswaran, D. A. Haber, Androgen receptor signaling in circulating tumor cells as a marker of hormonally responsive prostate cancer. *Cancer Discov.* **2**, 995–1003 (2012).
22. L. R. Huang, E. C. Cox, R. H. Austin, J. C. Sturm, Continuous particle separation through deterministic lateral displacement. *Science* **304**, 987–990 (2004).
23. D. Di Carlo, D. Irimia, R. G. Tompkins, M. Toner, Continuous inertial focusing, ordering, and separation of particles in microchannels. *Proc. Natl. Acad. Sci. U.S.A.* **104**, 18892–18897 (2007).
24. R. Huang, T. A. Barber, M. A. Schmidt, R. G. Tompkins, M. Toner, D. W. Bianchi, R. Kapur, W. L. Flejter, A microfluidics approach for the isolation of nucleated red blood cells (NRBCs) from the peripheral blood of pregnant women. *Prenat. Diagn.* **28**, 892–899 (2008).
25. G. Segré, A. Silberberg, Radial particle displacements in Poiseuille flow of suspensions. *Nature* **189**, 209–210 (1961).
26. A. M. Sieuwerts, J. Kraan, J. Bolt, P. van der Spoel, F. Elstrodt, M. Schutte, J. W. M. Martens, J. W. Gratama, S. Sleijfer, J. A. Foekens, Anti-epithelial cell adhesion molecule antibodies and the detection of circulating normal-like breast tumor cells. *J. Natl. Cancer Inst.* **101**, 61–66 (2009).
27. M. Yu, G. A. Smolen, J. Zhang, B. Wittner, B. J. Schott, E. Brachtel, S. Ramaswamy, S. Maheswaran, D. A. Haber, A developmentally regulated inducer of EMT, LBX1, contributes to breast cancer progression. *Genes Dev.* **23**, 1737–1742 (2009).
28. D. A. Haber, N. S. Gray, J. Baselga, The evolving war on cancer. *Cell* **145**, 19–24 (2011).
29. B. D. Plouffe, L. H. Lewis, S. K. Murthy, Computational design optimization for microfluidic magnetophoresis. *Biomicrofluidics* **5**, 13413 (2011).
30. W. J. Allard, J. Matera, M. C. Miller, M. Repollet, M. C. Connelly, C. Rao, A. G. Tibbe, J. W. Uhr, L. W. Terstappen, Tumor cells circulate in the peripheral blood of all major carcinomas but not in healthy subjects or patients with nonmalignant diseases. *Clin. Cancer Res.* **10**, 6897–6904 (2004).

Acknowledgments: We express our gratitude to all patients who participated in this study and healthy volunteers who contributed blood samples. We thank C. Koris and the MGH clinical research coordinators for help with clinical studies; B. Brannigan and H. Zhu for support of molecular analyses; E. Lim, J. Martel, J. Oakey, and F. Fachin for assistance in microfluidic device development; H. Cho for contributions to illustrations; L. Libby, O. Hurtado, and A. J. Aranyosi for coordination of the research labs; B. Hamza for expertise in device fabrication; D. Chianese and T. Bendele from Johnson & Johnson for supplying reagents and materials; and N. Bander from Weill Cornell Medical College for supplying anti-PSMA antibody, clone J591. **Funding:** This work was partially supported by NIH P41 Biotechnology Resource Center (M.T.), NIH National Institute of Biomedical Imaging and Bioengineering (M.T. and D.A.H.), Stand Up to Cancer (D.A.H., M.T., and S.M.), Howard Hughes Medical Institute (D.A.H.), Prostate Cancer Foundation and Charles Evans Foundation (D.A.H. and M.T.), Department of Defense Prostate Cancer Research Program (D.T.M. and R.J.L.), Mazzone-DF/HCC (Dana-Farber/Harvard Cancer Center) (D.T.M.), Conquer Cancer Foundation (R.J.L.), Prostate Cancer Foundation (R.J.L.), and Johnson & Johnson (M.T. and S.M.). **Author contributions:** E.O., A.M.S., B.L.E., D.T.M., E.B., M.Y., S.L.S., N.M.K., T.A.B., J.R.W., K.S., P.S.S., J.P.S., R.J.L., D.T.T., X.L., A.T.S., A.B., L.V.S., D.N.L., S.M., R.K., D.A.H., and M.T. designed the research. E.O., A.M.S., and J.C.C. were responsible for overall system design and characterization. B.L.E., A.K., and M.Y. optimized and performed cytology and ICC staining on slides. D.T.M. and J.T. executed single-cell micromanipulation and RNA analysis. S.S. conducted molecular detection of NSCLC patients. P.C., B.M., J.T., S.S., and J.C.C. executed chip operation and blood processing. N.M.K. completed characterization of cell plating chamber. E.O., P.C., and B.M. completed immunofluorescence staining, scanning, and enumeration. E.O., A.M.S., B.L.E., D.T.M., E.B., M.Y., S.L.S., N.M.K., L.V.S., S.M., R.K., D.A.H., and M.T. analyzed the research. E.O., A.M.S., B.L.E., D.T.M., S.M., R.K., D.A.H., and M.T. wrote the paper. **Competing interests:** MGH filed for patent protection for the CTC-iChip technology. The authors declare that they have no competing interests. **Data and materials availability:** Biotinylated anti-EpCAM mouse monoclonal IgG1 (clone VU-1D9), PE-conjugated anti-CK8/18 mouse monoclonal IgG1 (clone C11), PE-conjugated anti-CK19 mouse monoclonal IgG2a (clone A53-B/A2), APC-conjugated anti-CD45 mouse monoclonal IgG1 (clone HI30), nuclear staining reagent DAPI, and cell membrane permeabilization reagent saponin were obtained under a Materials Transfer Agreement from Johnson & Johnson (contact: David Chianese). Anti-PSMA monoclonal mouse IgG1 antibody (clone J591) was obtained under Materials Transfer Agreement from Weill Medical College (contact: Neil Bander).

Submitted 27 August 2012
Accepted 22 March 2013
Published 3 April 2013
10.1126/scitranslmed.3005616

Citation: E. Ozkumur, A. M. Shah, J. C. Ciciliano, B. L. Emmink, D. T. Miyamoto, E. Brachtel, M. Yu, P. Chen, B. Morgan, J. Trautwein, A. Kimura, S. Sengupta, S. L. Stott, N. M. Karabacak, T. A. Barber, J. R. Walsh, K. Smith, P. S. Spuhler, J. P. Sullivan, R. J. Lee, D. T. Ting, X. Luo, A. T. Shaw, A. Bardia, L. V. Sequist, D. N. Louis, S. Maheswaran, R. Kapur, D. A. Haber, M. Toner, Inertial focusing for tumor antigen–dependent and –independent sorting of rare circulating tumor cells. *Sci. Transl. Med.* **5**, 179ra47 (2013).